

**FABRICATION OF Lu DOPED YBCO THIN FILMS
BY PULSED LASER DEPOSITION TECHNIQUE
AND THEIR CHARACTERIZATION**

**A Thesis Submitted to
the Graduate School of Engineering and Sciences of
İzmir Institute of Technology
in Partial Fulfillment of the Requirements for the Degree of**

MASTER OF SCIENCE

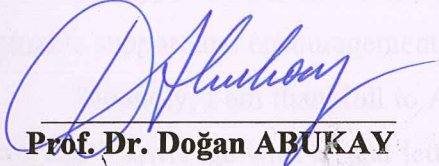
in Physics

**by
Bahtiyar Şirvan SEZER**

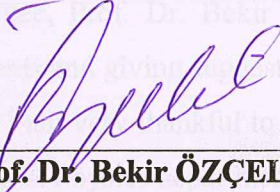
**December 2010
İZMİR**

We approve the thesis of **Bahtiyar Şirvan SEZER**

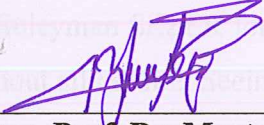
ACKNOWLEDGEMENTS



Prof. Dr. Doğan ABUKAY
Supervisor



Prof. Dr. Bekir ÖZÇELİK
Committee Member



Assoc. Prof. Dr. Mustafa TEPE
Committee Member

24 December 2010



Prof. Dr. Nejat BULUT
Head of the Department of Physics



Prof. Dr. Sedat AKKURT
Dean of the Graduate School of
Engineering and Sciences

ACKNOWLEDGEMENTS

Firstly, I would like to thank to my advisor Prof. Dr. Dođan ABUKAY, for his valuable support and encouragement in every part of this thesis.

Secondly, I am thankful to Assoc. Prof. Mustafa TEPE for sharing his valuable time and knowledge with us and letting us use the Superconductivity Laboratory at the Physics department of Ege University.

As well as my advisor, I would like to thank to the other members of my defence committee, Prof. Dr. Bekir ÖZÇELİK and Assoc. Prof. Mustafa TEPE for helpful comments and giving suggestions.

I am very thankful to Prof. Dr. Orhan ÖZTÜRK for helping XRD measurement at I.Y.T.E. Physics department.

I want to thank to IYTE Material Research Center staff for SEM, EDX, XRD and AFM analysis.

Finally, I would like to thank my dear family: my mother Tahire SEZER and my father Süleyman SEZER for their endless support, encouragement, motivation and love throughout all my life. Seeing them by my side for my whole life is the most important.

ABSTRACT

FABRICATION OF Lu DOPED YBCO THIN FILMS BY PULSED LASER DEPOSITION TECHNIQUE AND THEIR CHARACTERIZATION

Nearly twenty years ago YBCO was the first superconductor discovered with a transition temperature above the boiling point of liquid nitrogen, the “fascinating” limit for high temperature superconductivity. From the day forward, the interest in this ceramic compound has not diminished. YBCO is one of the most promising materials for the application of high temperature superconductors (HTS) because it is able to carry a technically useful current density in applied fields at 77 K. A lot of experiments guided to investigate the basic properties of the HTS and to further the theoretical understanding of them also used YBCO, because this progress has been achieved in the preparation of bulk samples, and especially thin films deposited by a various methods.

The aim of the experimental investigation presented in this thesis was to produce high quality epitaxial Lutetium doped YBCO thin films on MgO substrates prepared by pulsed laser deposition. For this purpose, bulk Lu_2O_3 powder was mixed into YBCO by using solid-state reaction method and pressed to make a stoichiometric target for PLD process. KrF excimer laser was worked at 14 Kv with repetition rates ranging from 3 to 5 Hz to deposited $\text{Y}_{0.9}\text{Lu}_{0.1}\text{Ba}_2\text{Cu}_3\text{O}_{7-\delta}$ thin films at a substrate temperature of 800 °C. The surface of the films were characterized by employing XRD, SEM, EDX and AFM techniques.

ÖZET

Lu KATKILI YBCO İNCE FİLMLERİNİN PULS-LAZER YIĞMA TEKNIĞİYLE YAPILMASI VE KARAKTERİZASYONU

Yaklaşık yirmi yıl önce YBCO yüksek sıcaklık süperiletkenliği için büyüleyici bir sınır olan sıvı azotun kaynama sıcaklığının üzerinde bir geçiş sıcaklığına sahip ilk süperiletken olarak keşfedildi. O zamandan beri, bu seramik bileşiğe olan ilgi artarak devam etmiştir. YBCO, yüksek sıcaklık süperiletkenlerin uygulama alanları için en umut verici materyallerden biridir çünkü 77K'de uygulanan alanlarda teknik bakımdan faydalı akım yoğunluğu taşıyabilme özelliğine sahiptir. Birçok deneysel çalışmada YBCO yüksek sıcaklık süperiletkenlerinin başlıca özelliklerinin araştırılmasına ve teorik olarak ifade edilmesine rehberlik etmiştir çünkü bu süreç bulk örnekler hazırlanarak, çeşitli metotlarla ince filmler kaplanarak sağlanmıştır.

Bu tezde sunulan deneysel araştırmanın amacı, MgO alttaşlar üzerine, puls-lazer yığma tekniğiyle, yüksek kaliteli epitaksiyel Lütelyum katkılu YBCO ince filmler üretmektir. Bu amaçla, bulk Lu_2O_3 tozu katı-hal tepkime yöntemiyle YBCO ile karıştırılmıştır ve PLD yöntemi için stokiyometrik target oluşturmak amacıyla preslenmiştir. $\text{Y}_{0.9}\text{Lu}_{0.1}\text{Ba}_2\text{Cu}_3\text{O}_{7-\delta}$ ince filmlerin kaplanması için KrF excimer lazer 3 ve 5 Hz'lik tekrarlama değerleriyle 14 Kv enerjide çalışmış, alttaş sıcaklığı da 800 °C'de tutulmuştur. Oluşan filmlerin yüzeyi XRD, SEM, EDX ve AFM analiz teknikleriyle incelenmiştir.

To my Family

For their endless support and encouragement

TABLE OF CONTENTS

LIST OF FIGURES	ix
LIST OF TABLES	xi
CHAPTER 1. INTRODUCTION.	1
1.1. Superconductivity	1
1.1.1. Historical Review	1
1.1.2. Basic Phenomena	2
1.1.3. Meissner Effect (Perfect Diamagnetism).....	3
1.1.4. The BCS Theory	5
1.1.5. Type I and Type II Superconductors	6
1.1.6. The Bean Critical State Model.....	8
1.1.7. High Tc Superconductors	9
1.1.7.1. Crystal Structure of YBa ₂ Cu ₃ O _{7-δ}	10
1.1.8. Issues for Substrate Selection for High-Tc Superconductors	14
1.1.8.1. Lattice Matching	14
1.1.8.2. Chemical Compability	15
1.1.8.3. Surface Quality	15
1.1.8.4. Thermal Stability	16
1.1.8.5. Thermal Expansion Match.....	16
CHAPTER 2. PULSED LASER DEPOSITION	17
2.1. Historial Development of PLD	17
2.2. Typical PLD set-up.....	18
2.3. Principles of PLD.....	19
2.3.1. Laser-Target Interaction	20
2.3.2. Laser-Plasma Interaction	22
2.3.3. Plume-Substrate Interaction.....	22
2.3.4. Particulate Formation.....	23
2.3.5. Choice of Independent Variables for Optimization.....	24
2.3.6. Film Growth Mechanism	25

2.4. YBCO Film Growth by Pulsed Laser Deposition	26
2.5. Advantages and Disadvantages of PLD.....	30
CHAPTER 3. EXPERIMENTAL.....	32
3.1. Lutetium Doped YBa ₂ Cu ₃ O _{7-δ} Target for PLD	32
3.1.1. Lutetium.....	32
3.1.2 Target Preparation.....	33
3.2. Substrate Preparation and Cleaning.....	34
3.3. Experimental Aspects of PLD	36
3.3.1. Laser and Laser Optics	36
3.3.2. Deposition Chamber and Pumping.....	38
3.3.3. Deposition Parameters	41
3.4. Characterization Techniques.....	43
3.4.1. Electrical Characterization.....	43
3.4.1.1. Resistance vs Temperature Measurements	43
3.4.1.1.1. Cryogenics	43
3.4.1.1.2. Electrical Contacts	44
3.4.2. Surface Characterization.....	45
3.4.2.1. X-Ray Diffraction (XRD).....	45
3.4.2.2. Atomic Force Microscopy (AFM).....	46
3.4.2.3. Scanning Electron Microscopy (SEM) and Energy Dispersive X-ray Spectroscopy (EDX or EDS).....	47
CHAPTER 4. RESULTS AND DISCUSSIONS.....	49
4.1. Structural Characterization	49
4.1.1. XRD Results	49
4.1.2. SEM and EDX Results	51
4.1.3. AFM Results	53
4.2. Electrical Characterization of Lu Doped YBCO Thin Films	54
4.2.1. Resistance vs Temperature Measurements.....	54
CHAPTER 5. CONCLUSION.....	56
REFERENCES	59

LIST OF FIGURES

<u>Figure</u>	<u>Page</u>
Figure 1.1. The evaluation of critical temperatures since the discovery of Superconductivity	2
Figure 1.2. The drop to zero resistivity	3
Figure 1.3. Meissner Effect	5
Figure 1.4. The formation of copper pairs	6
Figure 1.5. Type I superconductivity	7
Figure 1.6. Type II superconductivity	8
Figure 1.7. The structure of YBCO	11
Figure 1.8. Perovskite structure.....	12
Figure 1.9. Phase diagram of $\text{YBa}_2\text{Cu}_3\text{O}_{7-\delta}$	13
Figure 1.10. Oxygen content and T_c in YBCO.....	13
Figure 1.11. Epitaxial relationship between film and substrate	15
Figure 2.1. Schematic representation of PLD system.....	19
Figure 2.2. The schematic illustration for interaction of a target and laser pulse	20
Figure 2.3. The schematic diagram for atomic processes in the nucleation of the three dimensional clusters of deposited thin film atoms on a substrate surface	26
Figure 2.4. Film possible growths.....	26
Figure 2.5. Oxygen pressure and growth temperature phase diagram for the growth of YBCO using various techniques	28
Figure 2.6. Temperature vs. partial oxygen pressure phase diagram for YBCO according to Bormann and Nölting and Hammond and Bormann	29
Figure 3.1. Flowchart of YBCO.....	33
Figure 3.2. Lu doped YBCO target's diameters	34
Figure 3.3. Crstal structure of magnesium oxide	35
Figure 3.4. The optic system and vacuum chamber of PLD.....	37
Figure 3.5. A Neocera six target carrousel for in-situ multilayer deposition.....	39
Figure 3.6. PLD in our lab.....	40
Figure 3.7. Target and substrate holders.	40
Figure 3.8. Schematic illustration of the substrate on holder.....	42

Figure 3.9.	Deposition parameters	42
Figure 3.10.	The image of the plume during deposition	42
Figure 3.11.	R-T characterization setup in our lab.....	45
Figure 3.12.	2 Θ X-ray diffraction geometry for phase, composition and normal- to-substrate texture measurements.....	46
Figure 3.13.	A schematic diagram of an atomic force microscope (AFM)	47
Figure 4.1.	XRD result of Lu doped YBCO target	50
Figure 4.2.	XRD result of Lu doped YBCO thin film on MgO substrate.....	50
Figure 4.3.	EDX result of Lutetium doped YBCO target	51
Figure 4.4.	SEM for the films deposited at 800 oC, 300 mTorr and 14 kV.....	52
Figure 4.5.	Lu doped YBCO films had the same deposition parameters but these films were annealed at 670 oC for 30 minutes	53
Figure 4.6.	AFM surface roughness analysis of the Lu doped YBCO thin films on MgO substrates	54
Figure 4.7.	R-T measurement of the films that produced using (670oC, 300 Torr O ₂ , 30 min.) annealing process	55
Figure 4.8.	R-T measurement of the films that produced using (650oC, 250 Torr O ₂ , 45 min.) annealing process	55

LIST OF TABLES

<u>Table</u>		<u>Page</u>
Table 1.1.	The dimensions of the unit cell.....	12
Table 2.1.	Typical parameters taken from the literature.....	30
Table 3.1.	Typical properties of single crystal MgO substrates	35
Table 3.2.	Some of our tested deposition parameters and the ones in rectangle are successful ones.....	43

CHAPTER 1

INTRODUCTION

1.1. Superconductivity

In this section, an overview of superconductivity will be presented. In the first subsection, the historical review of the superconductivity will be mentioned. In the next subsection, Meissner effect, BCS theory, type I and type II superconductors, Bean critical state model and high- T_c superconductors will be explained in details.

1.1.1. Historical Review

The phenomenon of superconductivity was discovered by the Dutch physicist H. Kamerlingh Onnes in 1911. He found that dc resistivity of mercury suddenly drops to zero below 4.2 K.

In 1933, W.Meissner and R. Ochsenfeld discovered one of the most fundamental properties of superconductors: perfect diamagnetism. They found that the magnetic flux is expelled from the interior of the sample that is cooled below the critical temperature in weak external magnetic fields.

In 1934 F. and H. London discovered a simple two-fluid model. The London model explained the Meissner effect and predicted the penetration depth λ : a characteristic length of penetration of the static magnetic flux into a superconductor.

In 1957 John Bardeen, Leon Cooper and Robert Schrieffer proposed a complete microscopic theory of superconductivity. This is usually referred to as the BCS theory.

Then, in 1986, a truly breakthrough discovery was made in the field of superconductivity. Georg Bednorz and Alexander Müller researchers at the IBM Research Laboratory in Rüslikon, Switzerland, created a brittle ceramic compound that showed superconductivity at the highest then temperature known 30 K. Ceramics are normally insulators and do not conduct electricity well at all, so the researchers had not considered them as possible high-temperature superconductor candidates. This

property of ceramics made the discovery so remarkable. The Lanthanum, Barium, Copper and Oxygen ($\text{La}_{1.85}\text{Ba}_{0.15}\text{CuO}_4$) compound that Müller and Bednorz synthesized was the evidence for high- T_c superconductivity at ~ 30 K.

In February 1987 K. Wu and Paul Chu discovered $\text{Y}_1\text{Ba}_2\text{Cu}_3\text{O}_7$ ceramics with $T_c = 92$ K. This was an important discovery that for the first time a superconductor had a critical temperature above liquid nitrogen which is a much cheaper coolant than liquid helium.

Early in 1988, Bi- and Ti- cuprate oxides were discovered with $T_c = 110$ and 125 K respectively.

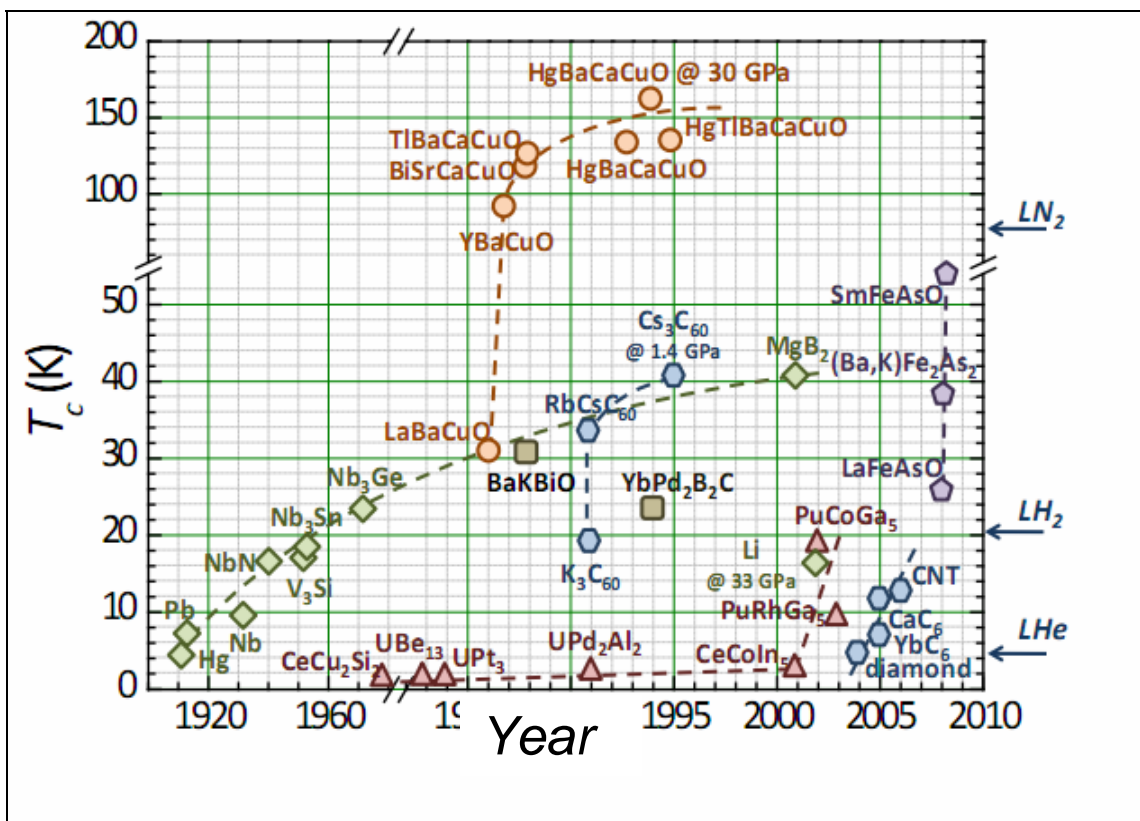


Figure 1.1. The evolution of critical temperatures since the discovery of superconductivity (Source: Gross and Hackl, 2001-2009)

1.1.2. Basic Phenomena

The electrical resistivity of all metals and alloys decreases when they are cooled. The resistivity of a superconductor vanishes abruptly at a certain temperature. The temperature at which superconductors lose resistance is called transition

temperature or critical temperature T_c . Below T_c ; it enters an entirely different superconducting state. Superconducting transition is reversible: when they heated it recovered its normal resistivity at the temperature T_c . At the temperature above absolute zero the atoms are vibrated and will be displaced by various amounts of from their equilibrium position furthermore foreign atoms or other defects randomly distributed can interrupt the perfect periodicity. Both the thermal vibrations and any impurities or imperfections scatter the moving electrons and give rise to electrical resistance. When the temperature is lowered, the thermal vibrations of the atoms decrease and the conduction electrons are less frequently scattered. Any real specimens of metals cannot be perfectly pure and will contain some impurity. Therefore the electrons, in additions to being scattered by thermal vibrations of the lattice are scattered by impurities.

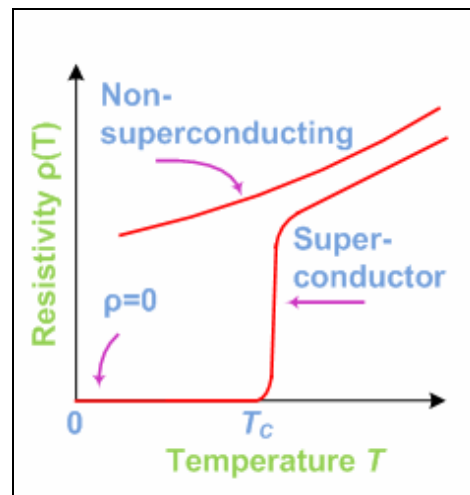


Figure 1.2. The drop to zero resistivity, $\rho = 0$, at a temperature T_c , compared to a normal behavior.

1.1.3. Meissner Effect (Perfect Diamagnetism)

Superconductors have unique combination of electric and magnetic properties. Although the term “superconducting” implies zero resistance, superconductors do not simply behave as perfect conductors ($R = 0$). In a perfect conductor the resistance around an imaginary close path is zero, therefore the amount of magnetic flux enclosed within this path cannot change. This must be true for any such imaginary circuit, which may happen only if the flux density at every point in the perfect conductor does not vary with time,

$$\frac{dB}{dt} = 0 \quad (1.1)$$

This means that if a perfect conductor at room temperature with no applied magnetic field is cooled to a very low temperature, and then a magnetic field is applied, the magnetic flux will not be allowed to enter the specimen and the interior will remain flux-free, since $dB/dt=0$ must hold.

On the contrary, if a perfect conductor is subjected to an applied field before the cooling, the flux density inside will be the same as that of the external field. This is due to the value of the relative magnetic permeability in most metals, which is very close to unity, except for the ferromagnetic materials. If the metal is then cooled down to a low temperature, this will have no effect on the magnetization, and the flux distribution will remain unchanged. Now, as the applied field is removed, dB/dt must hold again, so that currents will be induced in the interior of the perfect conductor, maintaining the flux inside unchanged, see Figure. 1.3.

In 1933, Meissner and Ochsenfeld measured the flux distribution of metal superconductors, cooled down to their T_c while in a magnetic field. They found out that a metal in the superconducting state never allows a magnetic flux density to exist in its interior. It exhibits perfect diamagnetism and the following equality always holds: $B = 0$. This property, which cannot be explained by an equivalence of superconductors with perfect conductors, has been named Meissner effect.

The expulsion of an applied field is a result of the existence of induced currents in a superconductor, which generate magnetic field, opposite in direction and equal in magnitude to the external field, so that the total field inside the superconductor is zero. The cancellation of flux lines within the superconductor may be viewed as if the external field lines are 'forced' to circumvent the specimen and not allowed to enter inside. The pattern of the external field depends on the shape of the specimen and is characterized by the demagnetizing factor η of the geometry. For superconductors of slab geometry in parallel field (thin rectangle with infinite length) the demagnetizing factor is zero. The state of perfect diamagnetism is retained only if the temperature is below T_c and the magnetic field below H .

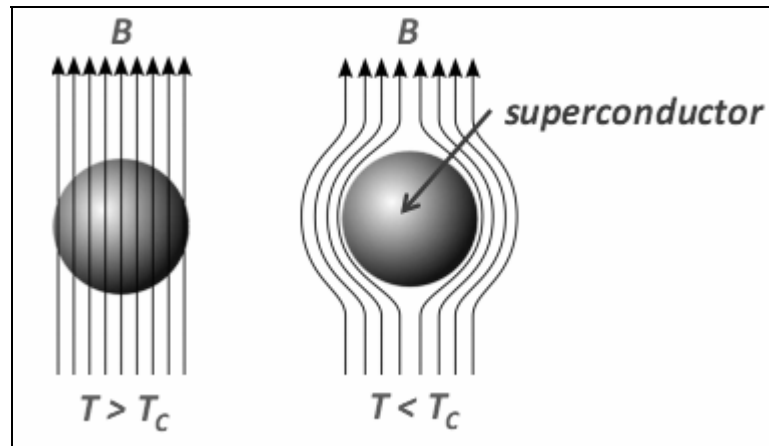


Figure 1.3. Meissner Effect
(Source: Gross , 2001-2009)

1.1.4. The BCS Theory

The microscopic mechanism of superconductor based on the effect of electron scattering was formulated by Bardeen, Cooper, and Schrieffer known as BCS theory in 1957. The BCS explains that atomic vibrations unify the entire current. As one negatively charged electron passes by positively charged ions in the lattice of superconductor, the lattice can distort. The distortion causes phonons to be emitted, which forms a rough of positive charge around electrons. The forces exerted by the phonons overcome the electrons repulsion and make them a pair known as cooper pairs. The Cooper pair could pass all the obstacles which caused resistance in the superconductors. Only if the superconductor is cooled to very low temperatures, the Cooper pairs can stay a pair due to the reduced molecular motion. However, once the superconductor gains heat energy, the vibration energy in the lattice become more increase and break the pairs. The distance between two electrons of the Cooper pair is defined as coherence length. The values for the coherence length range are from a few angstrom to as high as hundred nanometer (Figure 1.4).

Once the temperature of superconducting material is below the critical temperature, the resistivity of material is zero. The superconductor can hold huge current since there is no loss in electric energy when superconductors transmit electric current. However, there is a certain maximum current that the superconductor can carry. When certain amount of current is pushed through superconductors, it will relapse the superconductor to the normal metal state although the temperature is under its critical

temperature. The current value is called critical current density (J_c). An electrical current in a wire generate magnetic fields around a wire. The strength of the magnetic fields increase as the current in the wire increases, because superconductors are able to carry large current without loss of energy. The superconductors are well suited for making strong magnets, but the magnetic field also can relapse superconductors to normal metals known as critical magnetic fields (H_c).

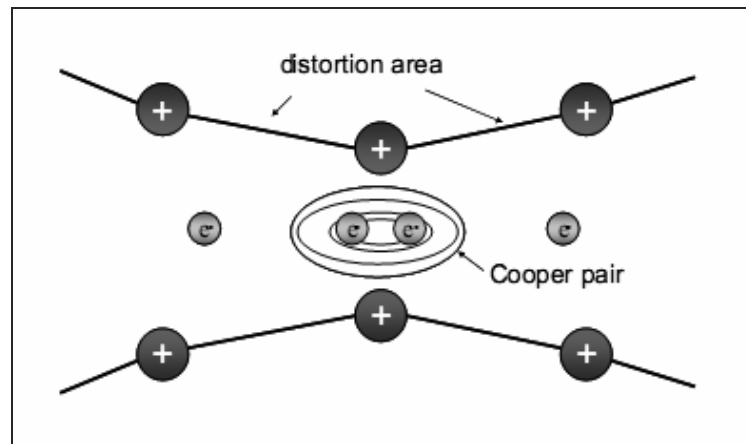


Figure 1.4. The formation of Cooper pairs; the two electrons become a pair together and could travel through the superconductor lattice. (Source: Kim, 2005)

1.1.5. Type I and Type II Superconductors

Superconductors are divided into two classes as Type I and Type II superconductors. In Type I superconductors there is no penetration of an external magnetic field into the material while it is in the superconducting state; $T < T_c$ and $H < H_c$. An applied external magnetic field only penetrates into the sample as much as the London penetration depth λ_L , as super currents are based on the outer part of the material, which build up a magnetization equal and opposite to the applied magnetic field. The Meissner effect, or perfect diamagnetism, was one of the two defining characteristics of a superconductor along with perfect conductivity. In Figure 1.5a the sample will be in the Meissner state below the superconducting region formed by the temperature and applied magnetic field, and in Figure 1.5b the internal magnetic field versus applied magnetic field (showed in another way). The internal magnetic field of the superconductor is zero up to the critical field H_c at which time the superconductor becomes normal and the magnetic field can penetrate the sample.

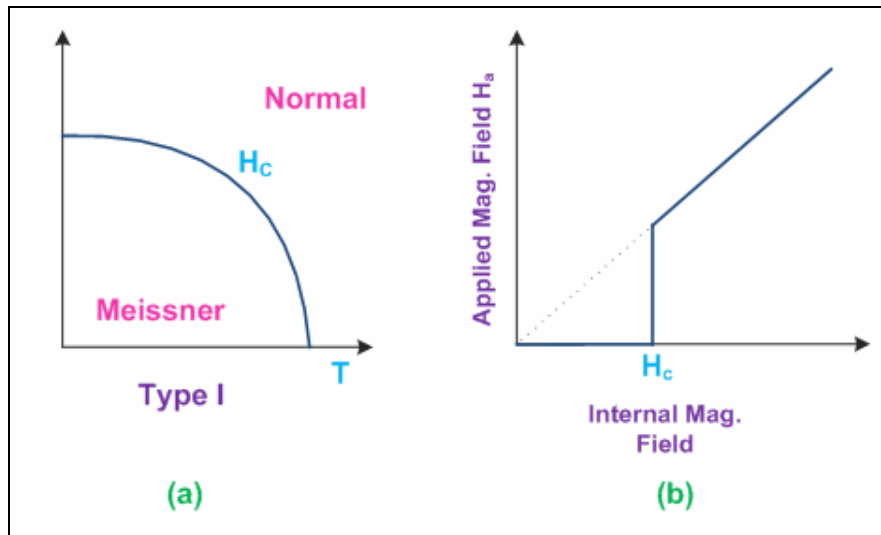


Figure 1.5. Type I superconductivity. (a) Penetration of the magnetic field into the sample in the normal state above H_c . (b) Behavior of the applied magnetic field versus internal field.

In the same year as BCS theory (1957), Alexi Abrikosov published a paper and introduced a new class of superconductors, which he termed these Type II superconductors. This new class of these new materials showed two distinct critical magnetic fields, H_{c1} and H_{c2} . The key feature of these was the penetration of magnetic flux into the material at a lower critical magnetic field H_{c1} . Below the lower critical magnetic field H_{c1} , the superconducting material behaves the same as a Type I superconductors, expelling the applied magnetic field. Notably, above the lower critical field and below the upper critical field, $H_{c1} < H < H_{c2}$, the material allows the penetration of the applied magnetic field in quantized vortices without the loss of superconductivity. Each vortex has a normal core that allows the magnetic field to pass through and is surrounded by a shielding super current, screening out the magnetic field locally, analogous to the screening of the bulk in Type I superconductors described above. An illustration of Type II superconductors is shown in Figure 1.6. Below H_{c1} is the usual Meissner state, like found in Type I superconductors. However, above H_{c1} but below H_{c2} , is the mixed state with magnetic flux penetration through the sample before coming to H_{c2} , above which superconductivity is destroyed and the sample becomes normal. The vortices are arranged in a regular lattice in the mixed state.

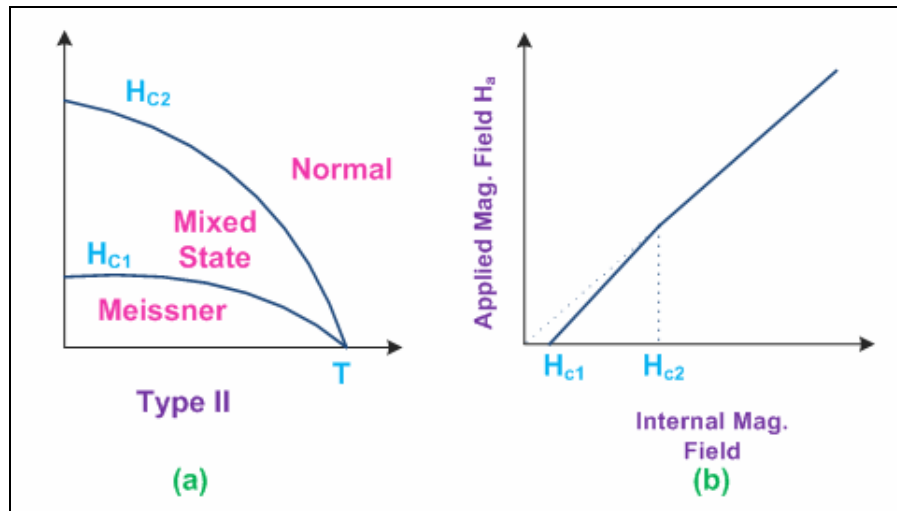


Figure 1.6. Type II superconductivity. **(a)** Type II superconductors have an additional phase between H_{c1} and H_{c2} , the mixed phase, that allows partial penetration of the magnetic field via flux lines. **(b)** Applied magnetic field versus internal field for Type II superconductors. There is no penetration until H_{c1} , after which there is partial flux penetration as vortices. The sample then becomes normal at H_{c2} .

1.1.6. The Bean Critical State Model

Modelling tools for HTS superconductors are required since theoretical solutions for current and field equations have been found for simple geometries only and are based on the assumptions of Bean's critical state model, which is not fully applicable to superconductors with smooth current-voltage characteristics. In this thesis we used only slab geometry so we will explain theoretical background of Bean model for slab geometry.

A great advance in the theoretical modelling of superconductors was triggered in 1957 by a paper from Abrikosov, who presented a theory for the magnetization of hard (Type II) superconductors, in which he showed that the flux enters the specimen in quantized flux lines, starting at very low field H_{c1} and completing its penetration at a much higher field H_{c2} . Several years afterwards, in order to obtain the virgin magnetization curves in hard superconductors, which exhibited magnetic hysteresis, Bean introduced a model, later referred to as the critical state model (CSM), a basic premise of which is the existence of a limiting macroscopic superconducting current density J_c that the superconductor can carry. In Bean's model only two states are possible to occur in the superconductor, zero current for regions with no magnetic flux

penetration, and full current with density J_c in regions with partial or complete flux penetration.

Along the width of a superconducting specimen, the current density is given by

$$J(x) = \begin{cases} 0, & H(x) = 0 \\ \pm J_c & H(x) \neq 0 \end{cases} \quad (1.2)$$

In Maxwell's Equation, this can be also written as:

$$\begin{aligned} \vec{\nabla} \times \vec{B} &= \mu_0 \vec{J} \\ \vec{\nabla} \times \vec{E} &= -\frac{\partial \vec{B}}{\partial t} \end{aligned} \quad (1.3)$$

with $J = \pm J_c$ or zero.

Even though experiments had shown that the critical current density is a function of the magnetic field, Bean assumed that J_c is independent of B , which in his early paper was equivalent to the assumption that the magnetic field is much less than the critical field of the filaments H_c .

1.1.7. High T_c Ceramic Superconductors

In 1986, Bednorz and Muller discovered superconductivity in LaBaCuO ceramics above the temperature limit postulated to be associated with the BCS theory. This report launched numerous studies worldwide and resulted in the discovery of many additional cuprate superconductors as shown in Figure 2.1. Indeed, at the special session of the 1987 fall MRS meeting in Boston, Paul Chu and coworkers defined a new record breaking the liquid nitrogen barrier (77K). The formula, $YBa_2Cu_3O_{7-\delta}$, (YBCO) was shown to exhibit superconducting properties at $\sim 92K$. This discovery is particularly important because these materials break the liquid nitrogen temperature, 77K. Before this time, it was most common for superconductors to be cooled with liquid helium (4.2K). Liquid helium cryogen is expensive to produce; it functions as an inefficient cryogen, and requires extensive safety precautions. Because this new class of superconductors had transition temperatures above the BCS theory predictions, they are called high temperature superconductors. Since 1987, several new formulas have been

discovered, raising the transition temperature to 135 K in ambient pressure and 160 K at elevated pressures.

Although many materials have been formulated which have transition temperatures above Paul Chu's formulation of YBCO, research is still being performed on this important material for a number of reasons. The YBCO materials can be transformed into axially oriented thin films useful for devices, which is more difficult with the superconducting materials that transition at a higher temperature. In addition, most of these higher transition temperature materials are inherently more toxic and include volatile components that complicate sample preparation and utilization. For example, the material with the highest transition temperature to date, $\text{HgBa}_2\text{Ca}_2\text{Cu}_3\text{O}_{1+x}$, ($T_c = 135$ K) requires heating in a sealed vessel so that gaseous mercury may intercalate into and remain within the crystalline lattice. Lastly, YBCO has regained renewed interest as it retains superconductivity under larger magnetic fields than many other superconductors in its class.

1.1.7.1. Crystal Structure of $\text{YBa}_2\text{Cu}_3\text{O}_{7-\delta}$

$\text{YBa}_2\text{Cu}_3\text{O}_{7-\delta}$ is a ceramic high temperature superconductor. Typical for this group of superconductors is their highly anisotropic layered structure built up of perovskite-like (ABO_3) subunit cells. In Figure 1.8 perovskite structure is illustrated. For YBCO the crystal structure exhibits a tripled unit cell of perovskite type. The crystal structure of YBCO can change depending on the oxygen stoichiometry. In Figure 1.7 the orthorhombic and tetragonal phases are shown. The orthorhombic unit cell contains two CuO_2 planes situated symmetric above and below the Y atom. It is in these planes that the superconductivity occurs. Each copper atom is surrounded by 5 oxygen atoms that form a pyramid with a basis area that is slightly distorted ($\approx 2\%$) from a square. There are also Cu atoms between the Ba atoms, which form Cu chains parallel to the b axis. These Cu atoms are only surrounded by 4 O atoms since the oxygen sites along the a-axis are not occupied. Further, the YBCO unit cell consists of three subunit cells, two containing a Ba atom and one which is situated in between them containing an Y atom.

The dimensions of the unit cell are seen in Table 1.1. The c-axis lattice constant is much larger than those for the other two lattice directions. The values for the

a- and b-axis are almost identical which leads to frequent formation of twin boundaries, since areas with different orientations can easily be formed by the crystal growth.

Depending on the oxygen doping, the crystallographic phase changes. Beside the superconducting orthorhombic phase also a tetragonal phase exists at low oxygen doping. The oxygen doping can be described by the parameter δ . For $\delta=1$ there is tetragonal $\text{YBa}_2\text{Cu}_3\text{O}_6$ which is an antiferromagnetic insulator. When δ is getting smaller a phase transformation occurs at $\delta=0.6$ into the orthorhombic phase. At the same time there is a phase transition from the antiferromagnetic insulator to the superconducting phase. Figure 1.9 shows the phase diagram for YBCO, which is typical for the cuprate high temperature superconductors. As seen in the phase diagram, at $\delta=0.05$ the superconductor has its highest transition temperature $T_c=92$ K. This $\text{YBa}_2\text{Cu}_3\text{O}_{6.95}$ is the optimally doped form of YBCO. With increasing δ , the transition temperature decreases and the system moves into the so called under doped regime. In the same way for decreasing δ also T_c decreases and the system moves into the over doped regime which is small since δ can not get negative. This can be understood by looking at the electronic structure of YBCO.

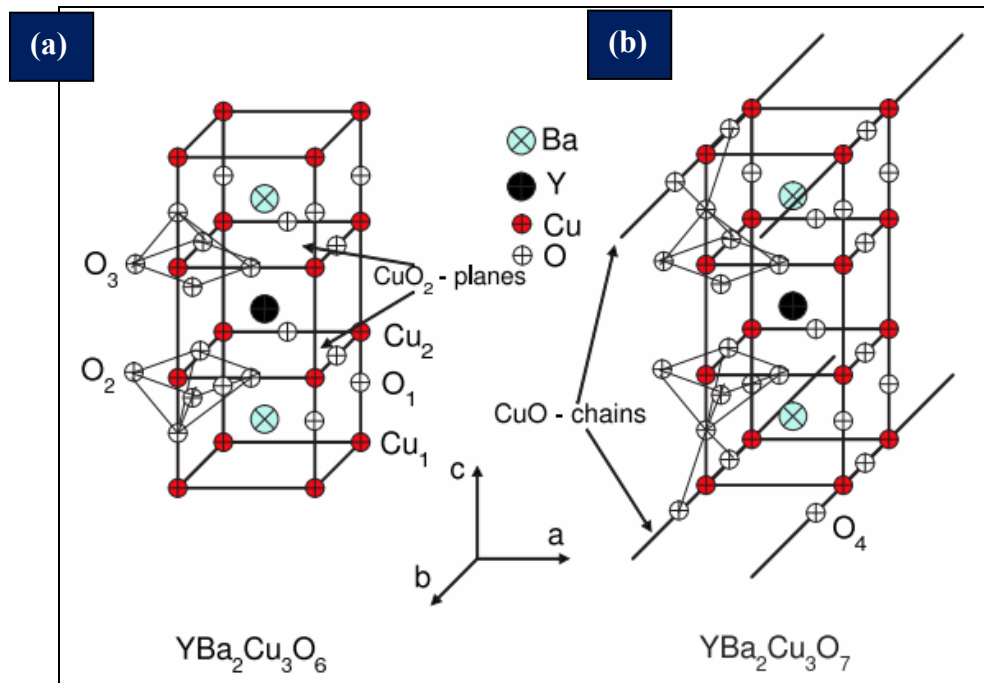


Figure 1.7. The structure of YBCO (a) tetragonal structure ($a_0 = b_0 = 3.86 \text{ \AA}$, $c_0 = 11.7 \text{ \AA}$) (b) orthorhombic structure ($a_0 = 3.823 \text{ \AA}$, $b_0 = 3.885 \text{ \AA}$, $c_0 = 11.7 \text{ \AA}$) (Source:Soltan, 2005)

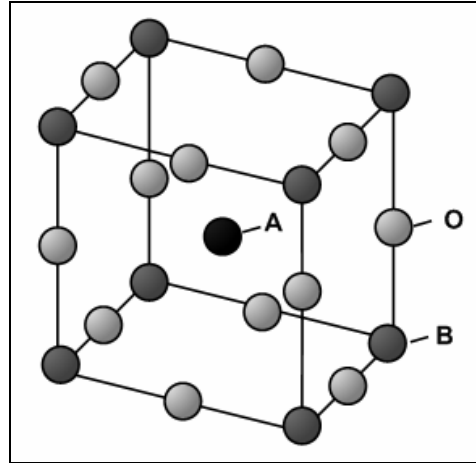


Figure 1.8. Perovskite structure.

Table 1.1. The dimensions of the unit cell.

<i>a</i>	<i>0.3814 nm</i>
<i>b</i>	<i>0.3884 nm</i>
<i>c</i>	<i>1.1660 nm</i>

Important for superconductivity are the CuO_2 planes that are situated symmetrically on both sides of the Y^{3+} ion, and the one dimensional Cu-chains situated between the Ba^{2+} ions. The fully doped compound is $\text{YBa}_2\text{Cu}_3\text{O}_7$ where all the oxide sites are filled. With increasing δ more and more oxide atoms leave the oxide chains until at $\delta = 1$ they are completely extinguished. The CuO_2 -planes always remain fully occupied. Owing to the strong electro-negativity of the oxygen, occupation of the oxide sites in the copper chains leads to a transfer of electrons from the planes into the chains. Thus with a decreasing δ , a stronger hole doping in the planes is achieved. These holes are those for the superconductivity relevant charge carriers. In this way, an increasing δ lead to a reduction of charge carriers and, thus, also the superconducting properties like the transition temperature are reduced.

Since superconductivity takes place in the two-dimensional CuO_2 -planes, there is an extreme anisotropy of the material properties in these compounds. This anisotropy is reflected in the important superconducting parameters. The penetration depth, $\lambda_c = 700\text{--}800$ nm is much larger than $\lambda_{ab} = 140\text{--}160$ nm and the coherence length, $\xi_{ab} = 1.0\text{--}2.0$ nm larger than $\xi_c = 0.3\text{--}0.4$ nm. The coherence length along the c-direction shows roughly the same value as the distance between the CuO_2 -planes. This leads to a suppression of the density of Cooper pairs between the planes.

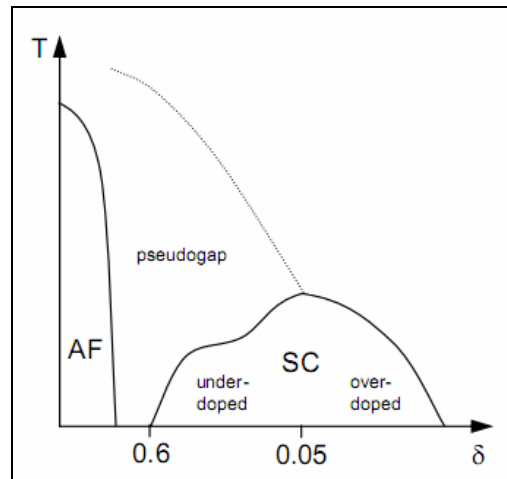


Figure 1.9. Phase diagram of $\text{YBa}_2\text{Cu}_3\text{O}_{7-\delta}$. Depending on oxygen doping δ and temperature the system can show antiferromagnetic, metallic or superconducting properties. (Source: Djupmyr, 2008)

As mentioned above, the electrical properties of all the high- T_c materials are strongly dependent on the number of charge carriers in the CuO_2 planes. Doping levels between 1.6 and 2.0 holes per copper in the planes promotes the highest T_c . Varying the oxygen content in these planes can alter the carrier concentration. This plays a large role in the synthesis of YBCO thin films. Two plateau's in the T_c vs. oxygen curve can be seen in Figure 1.10. With increasing oxygen content the first plateau is a T_c of 60 K at an oxygen content between 6.4 and 6.6. With higher oxygen content of 6.8 to 7.0 the T_c increases to it's highest level of 92 K.

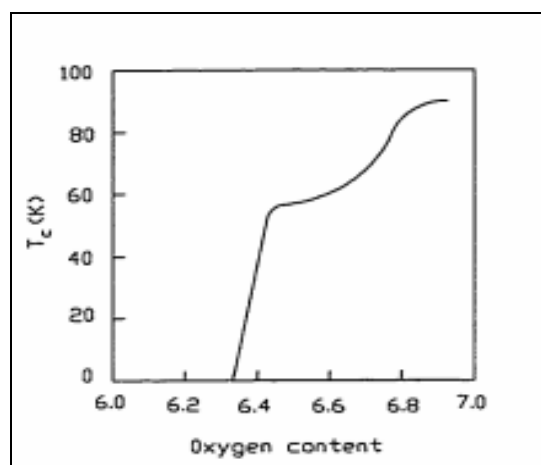


Figure 1.10. Oxygen content and T_c in YBCO (Source: Chudzik, 2000)

1.1.8. Issues for Substrate Selection for High- T_c Superconductors

The quality of film-substrate epitaxy is also strongly influenced by the differences in thermal expansion, chemical compatibility between the materials, surface quality, cleanliness, and homogeneity. When creating a multilayer device or only a structural template for a final layer, it is important to inhibit chemical reactions between layers. One must be conscious of the diffusivity of species involved at the growth temperatures in a range of 600-1000 °C for several hours during the deposition of following layers.

There are a lot of possible substrate choices for high temperature superconductors. The major issues involved in substrate selection include the following.

1.1.8.1. Lattice Matching

The highest quality films as determined by crystallography and transport measurements are obtained when the film is epitaxially grown from the underlying substrate. When the atomic sites between the two layers are brought into coincidence or near coincidence by either a rotation of crystal axis or straight cube-on-cube growth. This condition will only occur when the lattice constants are within 15 % each other. A better lattice match will mean higher quality films can be grown at lower substrate temperatures, because a lower number of misfit dislocations are required to make up the difference in atomic layer distances between the films.

Epitaxy is the growth or deposition of a film on a substrate such that the film has a certain crystallographic relationship to the substrate. It is important in that it allows for the reduction of defect densities and impurities as well as allows for the fabrication of multilayers with differing chemical, physical and electrical properties than substrate.

There are two types of epitaxy: homoepitaxy and heteroepitaxy. The latter refers to the growth of a film, or epilayer, on a substrate of similar material, for example the growth of silicon on silicon wafer. Heteroepitaxy refers to the growth of a film on a substrate of dissimilar material. An important example in superconducting applications is the growth of cerium oxide on yttria-stabilized zirconia.

Homoepitaxy results in a perfectly latticed matched multilayer because the epitaxial layer, called epilayer, and the substrate are the same material. Heteroepitaxy is the more technologically important and is far less trivial than homoepitaxy. Heteroepitaxy can result in one of the three epitaxial relationships illustrated in Figure 1.11 matched, strained or relaxed, depending on the mismatch in lattice parameters and thickness of the epilayer. If the mismatch is small enough the epitaxial relationship is the same as the homoepitaxy case where the layers are matched. If the mismatch is large then the epilayer will result in a strained or relaxed configuration.

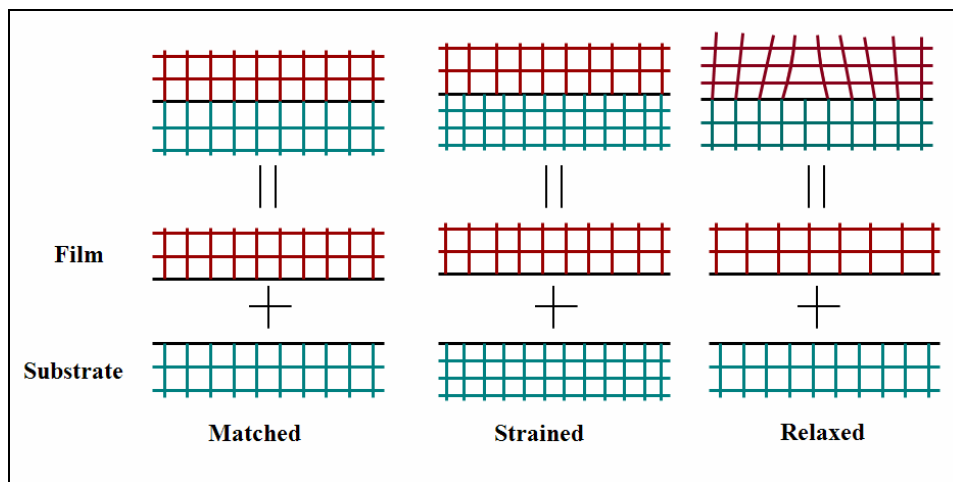


Figure 1.11. Epitaxial relationship between film and substrate.

1.1.8.2. Chemical Compatibility

It is important that the superconducting film does not react chemically with the buffer layer at the high deposition temperatures required to obtain epitaxy. This is whether true the film is epitaxial or not. The substrate must be unreactive in the oxygen rich deposition environments common with the metal-oxide buffer layers and superconductors.

1.1.8.3. Surface Quality

A smooth growth surface is paramount to obtaining high quality film. Some of the surface defects that effect film growth include:

- ❖ The sub-micron scale: impurity phases;

- ❖ The micron scale: pores, crystalline boundaries, grinding scratches;
- ❖ The micron scale: surface warp and cracks

Surface scratches can have a significant impact on nucleation processes. Surface quality plays a large role in film to film growth reproducibility.

1.1.8.4. Thermal Stability

The substrates and buffer layers used in superconducting film growth must be thermodynamically stable within the range of processing temperatures. In the case of zirconia substrates it is important that the cubic phase is stabilized within the temperatures used for YBCO growth.

1.1.8.5. Thermal Expansion Match

A large mismatch in the thermal expansion coefficient can lead to film cracking and possibly delamination during thermal cycling to and from film deposition temperatures.

CHAPTER 2

PULSED LASER DEPOSITION

Pulsed Laser Deposition (PLD) is a physical vapor deposition (PVD) technique based on the evaporation of material by using a pulsed, highly energetic laser beam focused inside a vacuum chamber to strike a target of the desired composition. This versatile technique may be applied to profoundly different materials such as, metals, insulators, semiconductors and high- T_c superconductors. With the use of PLD, the stoichiometric transfer of these materials from a multicomponent target to a film on a substrate can be obtained entirely. Under the right experimental conditions, PLD also offers the potential for epitaxial thin film growth.

2.1. Historical Development of PLD

After laser was first illustrated in 1960, it has used as a powerful and controlled energy source in many applications with its distinctive properties such as narrow frequency bandwidth, coherence and high power density. The first proof of the idea for using a laser tool to deposit thin films was carried out by Smith and Turner using a ruby laser in 1965. This was the very beginning of the development of pulsed laser deposition technique. Then, Venkatesan tried to use laser to deposit thin film of high- T_c superconductor YBCO, however, the elements in the composition of YBCO evaporated at different times due to the different rates and as a result, different composition from the target that was non-stoichiometric.

However, the development and investigations of PLD did not acquire the expected momentum. In fact, the availability of the types of laser was limited; the stability output was poor and the laser repetition rate was too low for any practical film growth processes.

In the late 1970's excimer lasers became available. These lasers provided both high energy density and ultraviolet (UV) wavelengths, allowing the disassociation of even very stable chemical bonds.

In 1987 Dijkkamp deposited the first thin film of a high- T_c superconductors by PLD using an excimer laser and, unlike Venkatesan, he achieved to deposit PLD growth thin film with the same stoichiometry as in the target.

The present name, pulsed laser deposition (PLD), was defined by formal voting from the participants of the first Material Research Society Symposium on Pulsed Laser Ablation held in San Francisco in April 1989.

During the last decade, PLD has been employed to fabricate crystalline thin films with epitaxy quality. Ceramic oxide, nitride films, metallic multilayers, and various superlattices grown by PLD to synthesis nanotubes, nanopowders and quantum dots have also been reported.

2.2. Typical PLD Setup

The basic idea of PLD can be simply explained by the experimental setup in Figure 2.1.

PLD system basically consists of a target holder and substrate holder in the vacuum chamber with a laser outside. The chamber is equipped with a UV (ultraviolet) transparent lens focuses the laser beam onto the target surface. The evaporation power source, i.e. the laser, is separated from the vacuum system, and this makes the technique very flexible.

The useful range of laser wavelengths for thin film growth by PLD lies between 200nm and 400nm. The growth can be occurred in ultra high vacuum or in the presence of a background gas, such as oxygen which is commonly used during the deposition of oxides to fully oxygenate the deposited films. Typically, each laser pulse has a duration length of a few nanoseconds.

Targets in PLD, usually in disk shape, are normally rotated and scanned with respect to the laser beam in order to suppress surface roughening. The most commonly used targets are ceramic ones. Dense small-grained targets are more desirable because single-crystalline or coarse-grain-polycrystalline ones are damaged by thermal shock after few pulses.

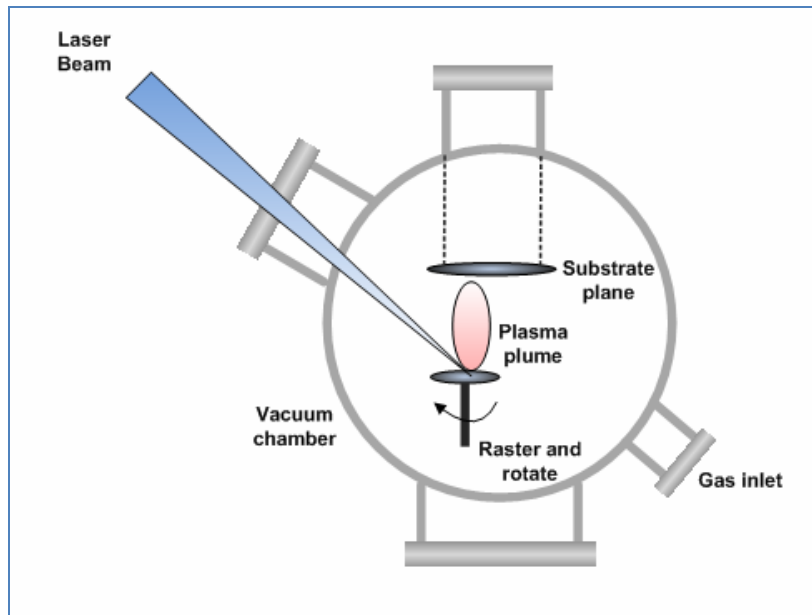


Figure 2.1. Schematic representation of PLD system

2.3. Principles of PLD

In this technique a pulsed high energetic laser beam is focused on a target resulting in ablation of material. At the early stage of the laser pulse a dense layer of vapor is formed in front of the target. Energy absorption during the remainder of the laser pulse causes, both, pressure and temperature of this vapor to increase, resulting in partial ionization. This layer expands from the target surface due to the high pressure and forms the so-called plasma plume. During this expansion, thermal and ionization energies are converted into the kinetic energy (several hundreds eV) of the ablated particles.

The theoretical description of PLD is highly complicated and draws on many disciplines of science. To understand this technique, the discussion of laser-target interaction, the laser-plasma interaction, the plume-substrate interaction, particulate formation, choice of independent variables and the film growth may be convenient. These six stages affect the quality and composition of the film grown.

2.3.1. Laser-Target Interaction

As illustrated in Figure 2.2 a simple physical description for the laser-target interaction in which material is removed from the target by several processes.

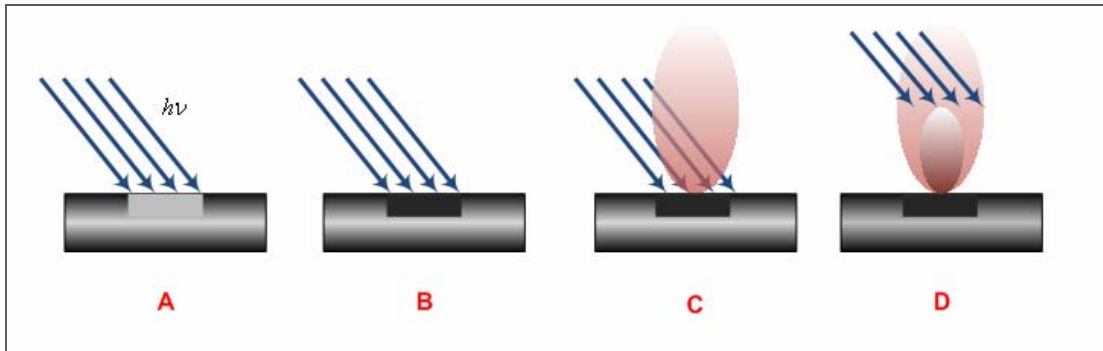


Figure 2.2. The schematic illustration for interaction of a target and laser pulse. (A) initial laser irradiation hits the laser. (B) it melts the surface of the target. (C) The liquid is vaporized. (D) then it is ionized to form a plasma which is ejected from the target surface.

In an extremely simplified picture, the laser ablation of a solid target occurs when the local temperature increased by means of the laser beam, overcome the vaporization temperature of such material. A number of parameters like the absorption coefficient and reflectivity of the target material, and the pulse duration τ , wavelength λ and laser fluence F (energy for pulse on spot size) affect the interaction of the laser beam with the target. Each material has its own threshold fluence F_{th} : for values of F above F_{th} the laser-target interaction regime is called ablation. For fluence values F lower than F_{th} the regime is called desorbing, for F higher than F_{th} it is called spallation.

From analytical point of view, the problem of laser–target interaction is very complex: the presence of a moving laser-solid interface, resulting from the melting and the evaporation, and the thermal dependence of the sample optical and thermal properties on the temperature, make extremely complicated the exact description of the phenomenon.

For this reason it is widely used a macroscopic approach, based upon an energetic balance: the problem is transformed in the calculus of the temperature distribution on the sample, after the interaction with laser radiation.

The target region concerned by the ablation process has the xy sizes of the laser spot dimension on target surface, times a L_{th} dimension, on the z direction perpendicular to the target. Such value of L_{th} depends on the thermal diffusivity of the sample material and on the pulse duration as followed:

$$L_{th} = \sqrt{2D\tau_L} \quad (2.1)$$

D is the thermal diffusivity and τ_L is the pulse duration. From hence, the longer the pulse, the deeper and the wider is the laser affected zone.

Since the value of L_{th} is usually very much smaller than the laser beam irradiated zone on the target surface (with a ns laser pulse $L_{th}=1\mu m$), one can assume that the thermal gradient in the transverse plane xy of the target face is irrelevant with respect to the thermal gradient in z direction normal to the target. In this approximation, the temperature distribution $T(r,t)$ into the irradiated target is given by the one dimensional heat equation.

In general the interaction between the laser radiation and the solid material occurs through the absorption of photons by electrons of the atomic system. The absorbed energy causes electrons to be in excited states with high energy and as a result heat the material up to very high temperatures in a very short time. Then, the electron subsystem will transfer the energy to the lattice, by means of electron-phonon coupling.

In this frame, the temporal and spatial evolution of the electrons subsystem and the lattice should be described by means of two different temperatures: T_e (electrons) and T_i (lattice), on the base of the two temperature diffusion model, developed by Anisimov et.al.

Nonetheless, in case of ns laser pulses, it can be assumed that $T_e=T_i=T$ since the electron-phonon coupling occurs in picoseconds time scale (typically 1–5ps). With the previous approximation, the ablation process via a ns laser pulse can be described by the one dimensional heat equation in T :

$$C_i \frac{\partial T}{\partial t} = \frac{\partial}{\partial z} \left(k_0 \frac{\partial T}{\partial z} \right) + \alpha A I(t) e^{-\alpha z} \quad (2.2)$$

Here, C_i is the heat capacitance of the lattice, $I(t)$ is the laser pulse intensity, k_0 is thermal conductivity and α is the absorption coefficient.

2.3.2. Laser-Plasma Interaction

In the description of the laser–plasma interaction, the laser pulse duration plays a critical role: although in the case of nanosecond laser pulse, the forming plasma interacts with the laser beam "tail", in the case of femtosecond (fs) laser pulse the previous mechanism doesn't take place.

The laser absorption of the forming plasma reduces the efficiency of the energy deposition into the sample (plasma shielding effect) and increases the plume ionization degree, complicating the plume expansion mechanism. Because of the plasma-laser interaction, the temperature of the evaporated material increases therefore rapidly to extremely high values and the electrons are further accelerated. The excited particles will emit photons, leading to a bright plasma plume, which is characteristic for the laser ablation process. The main absorption processes are the inverse bremsstrahlung (IB) and the photoionization (PI), since the cross section of the other processes are much smaller.

2.3.3. Plume-Substrate Interaction

In pulsed laser deposition, the deposition of the ablated material on the substrate surface can be regarded as instantaneous for every pulse, since the time scale of the atomistic processes involved in the film growth exceeds the deposition pulse duration. Each instantaneous deposition is followed by a relative long time interval, where no deposition occurs. Due to the instantaneous deposition at typical PLD conditions, the nucleation takes place after the deposition pulse and can be considered as post-nucleation. Such separated random deposition and subsequent growth is,

furthermore, advantageous for the study of the effect of plume expansion dynamics on film growth kinetics developed in this work.

Parameters which control the instantaneous deposition rate are the laser energy density at the target, the distance between target and the substrate and ambient gas properties, i.e. , pressure.

The extremely high deposition rate, typical of PLD deposition (of the order of 10^{20} atoms $\text{cm}^{-2} \text{s}^{-2}$), leads to a very high degree of supersaturation, $\Delta\mu$, defined as:

$$\Delta\mu = k_B T \ln \frac{R}{R_0} \quad (2.3)$$

k_B is the Boltzmann's constant, R is the actual deposition rate and R_0 its equilibrium value at temperature T .

Two independent process play a role during the vapor-phase epitaxial growth on a surface: the nucleation and the growth of islands. Both processes occur far from the thermodynamic equilibrium and are determined by kinetic processes. In the frame of the thermodynamical approach, used to describe the crystal growth close to equilibrium (for a thermodynamically stable system), local fluctuation from equilibrium leads to the phase transition from gas to solid, where a prerequisite for this process of nucleation is a supersaturated gas.

The high supersaturation of the vapor leads to a large nucleation rate. The nuclei will be formed until a critical density is reached. From this point on wards the nuclei will grow and crystallization process will occur.

2.3.4. Particulate Formation

Process conditions and deposition materials determine the generation rate, energy, velocity, size, chemistry, and microstructure of particulates deposited by PLD. Particulates have two main causes, but are saperated into four classes.

Three classes of particulates are due to laser-target interactions. The first type is caused by protrusions on the target surface, such as pits, craters, or microcracks, being mechanically dislodged from target due to laser-induced thermal and mechanical shock. This process is termed exfoliation. The second type of particulates is caused by

rapid expansion of trapped gas bubbles beneath the surface during laser irradiation, causing forcible ejection of molten surface matter by the process called subsurface boiling. The third type results from rapid surface evaporation splashing the molten layer left on the target. This is termed expulsion of the liquid layer by shock wave recoil pressure.

Target resurfacing before deposition, target densification, and target rotation minimize exfoliation. Reducing laser energy limits subsurface boiling as well as expulsion of the liquid layer by shock wave recoil pressure.

The last type of particulate matter is due to plume interactions. These particulates are created from the condensation of vapor species due to interplume collisions. To minimize this type of particulate, precise control must be obtained of the partial pressure of background gas used during the deposition. Reducing the pressure of ambient gas, reduces collisions between species in the plume and gas molecules, causing a reduction in the number density of condensation particulates.

A certain pressure of background gas, O_2 , is required during deposition to incorporate oxygen within YBCO. Pressures must be precisely controlled to allow the formation of film precursors within the plume without the creation of particulate matter.

2.3.5. Choice of Independent Variables for Optimization

Based on previous discussion of thin film deposition via pulsed laser ablation, there are a number of variables that effect deposition in a strong manner. The background pressure of oxygen incorporates oxygen in the lattice and creates particulate matter. The substrate temperature effects the mobility of species on the surface of substrate determining if the assembly recrystallizes into the desired phase. The laser energy determines the initial energy and velocities of the species in the plume. In addition, the laser energy can create laser droplets and influence film morphology by creating subsurface boiling or expulsion of the liquid layer by shock wave recoil pressure. The target to substrate distance determines the energy of species in the plume when they reach the target surface. The repetition rate of laser determines how often new material is delivered to the surface, which in turn defines the time period over which diffusing may occur prior to the arrival of the next layer.

2.3.6. Film Growth Mechanism

The thin film growth can be explained by three different modes such as three-dimensional island growth, two-dimensional monolayer formation, and the growth of separate islands on the top of a full monolayer. The three-dimensional film growth includes a number of processes that particles can go through after arriving on the substrate (Figure 2.3). The nucleation rate of the clusters and the relation of a cluster growth and dissociation are controlled by the total free energy of the system. The size of a stable cluster decreases with decreasing the surface energy between the arriving atoms and the clusters or increasing the negative volume free energy. In practice, changing the substrate temperature or increasing the deposition rate can control the free energy. A monolayer can be formed with low surface energy of the clusters and high surface energy of the substrate due to energy favor for the thin film. A higher temperature and a lower deposition rate support the formation of larger islands instead of numerous small clusters. Two-dimensional layers could be formed before three-dimensional nucleation. However, the growth mode changes from initial state to three-dimensional nucleation state because the increasing film thickness causes the stress due to lattice mismatching or strong relation between the substrate and the films.

In general, the quality of the deposited film is determined by the crystallinity of the lattice and the surface smoothness. The generation of particulates during the PLD process is one of the most important factors which can affect the smoothness of the films and crystallinity. These particulates can be classified as small droplets and large irregular shape outgrowths. The density of all kinds of particulates increases with the number of laser pulses because the largest outgrowths are believed to originate directly from the target. The typical explanation for large target fragments on the substrate is that the breaking of projecting surface features or splashing of a molten surface layer. However, the droplets are considered as resolidified molten drops from hydrodynamic sputtering of the target. Moreover, the loss of epitaxy in thicker films generates many types of differently shaped outgrowths. Precipitates are particles whose stoichiometry is different from that of the surrounding film. The crystallinity of the film is improved when precipitates are formed since the film is separated into two phases including the precipitates and the crystal matrix. In Figure 2.4 the possible film growth modes are illustrated.

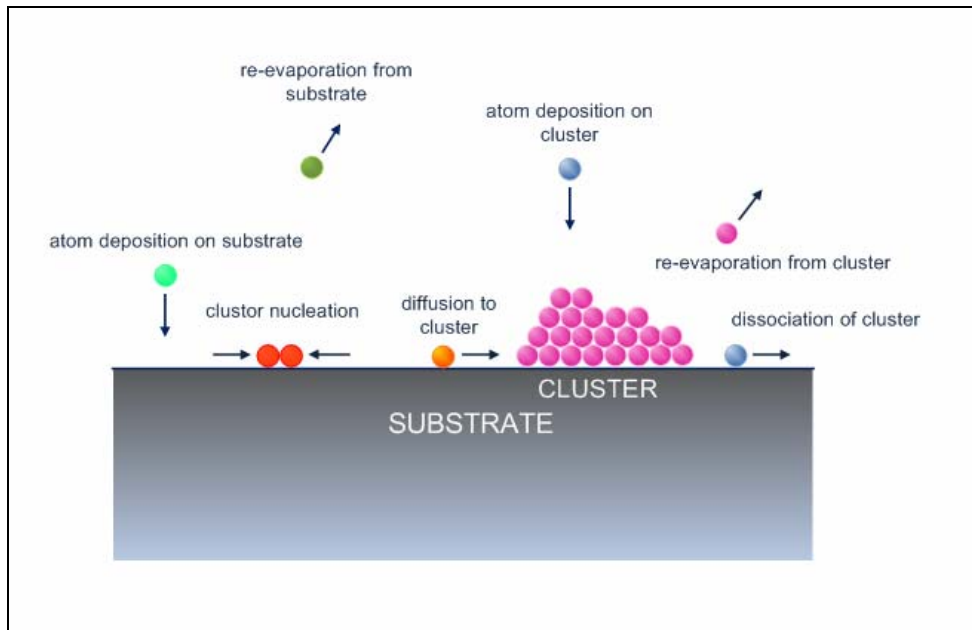


Figure 2.3. The schematic diagram for atomic processes in the nucleation of the three-dimensional clusters of deposited thin film atoms on a substrate surface.

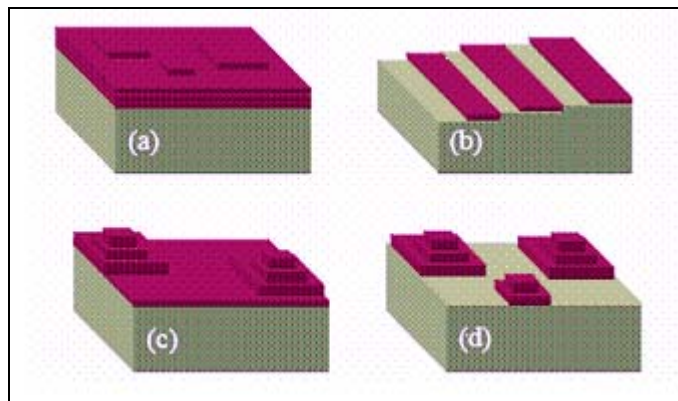


Figure 2.4. Film possible growths: **(a)** Frank-VanderMerwe layer-by-layer growth, **(b)** step-flow growth, **(c)** Stranski-Krastanov growth, **(d)** Volmer-Weber growth.

2.4. YBCO Film Growth by Pulsed Laser Deposition

The growth of high quality YBCO thin films is complicated by its complex composition, layered structure and limited thermodynamic stability of YBCO that complicates its growth. The oxygen- temperature thermodynamic phase diagram from the growth of the YBCO is given in Figure 2.5.

YBCO with 1-2-3 composition is only stable in a portion of the pO_2 -T phase diagram. Above, m_1 in Figure 2.5, YBCO incongruently melts. Below d_1 on the phase diagram YBCO decomposes into three separate phases, $BaCu_2O_2$, Y_2BaCuO_5 , and $YBa_3Cu_2O_{7.6}$. Line d_2 is another decomposition line that doesn't play a large role in film growth because it occurs at a low enough temperature that atom mobility is too low for thermodynamically more favorable phases to form. This line however forms a lower temperature limit for stable YBCO synthesis.

YBCO grown at high temperatures has an oxygen content between 6.0 and 6.3 which is a tetragonal phase and is not superconducting. By oxidation and cooling through temperatures around 650°C , YBCO becomes orthorhombic. This oxidized phase is superconducting and has room temperature a and b lattice parameters of approximately 3.83 \AA , and 3.88 \AA respectively. Although the phase is orthorhombic, the crystal structure is considered pseudo-tetragonal because of the nearly equal a and b lattice parameters. The superconducting transition temperature of this orthorhombic phase is near 92 K. The thermodynamic stability relationship in Figure 2.5. are actually significantly simplified and don't include the two orthorhombic phases I and II, which have different T_c 's depending on oxygen content, and are common in YBCO growth.

In-situ growth of YBCO is typically achieved at temperatures greater than 650°C because of the strong metal-oxygen bonds in YBCO, requiring high temperatures to provide enough adatom mobility to achieve epitaxial growth. Figure 2.5 includes reported pO_2 and temperatures zones for in-situ growth of YBCO by MOCVD, PLD, EBE, and sputtering.

As will be discussed in the next chapter, the first PLD pattern superconducting YBCO film presented by Dijkkamp et.al. in August 1987, in the same year that the discovery of YBCO by Wu et.al., with a T_c of $\sim 92 \text{ K}$, close to its bulk values. Before this success, the researchers had failed to catch the right stoichiometry of the film as its bulk samples. This provide the necessary incentive for many other research workers and they succeeded in depositing different kinds of complex oxide materials in the following few years.

Generally, near UV and visible lasers ($190 \text{ nm} \leq \lambda \leq 532 \text{ nm}$) seem to be ideal for the ablation of complex oxide materials, as they are able to generate a congruent material transfer from the ablation target to substrate, thereby ensuring the correct stoichiometry of growing film.

In most cases in PLD process, as-grown films are oxygen deficient and need to be annealed in higher pressures to develop their best superconducting properties. Here, the reported procedures differ even more than for the growth process itself. The general consensus seems to be that oxygen pressures up to 1 bar should be introduced as soon as possible after growth while the substrate is slowly cooling down. During the cool down, the temperature is often fixed at certain values for prolonged periods.

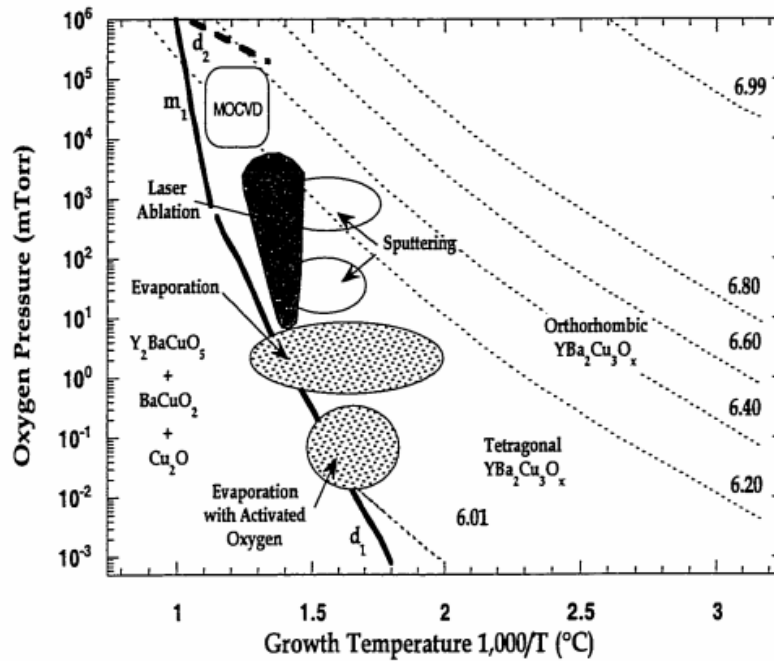


Figure 2.5. Oxygen pressure and growth temperature phase diagram for the growth of YBCO using various techniques. (Source: Chudzick, 2000)

Unfortunately, this fairly consistent understanding of the film growth does not define a sufficiently accurate procedure to achieve reliable results. Due to the very rich phase diagram of YBCO, its growth is very sensitive to small changes in the deposition conditions. Furthermore, each PLD apparatus has its unique characteristics, and growth parameters may not easily be transferred from one system to another. Therefore, the precise control and careful calibration of all parameters is necessary for each system, and finding the correct conditions is often a very time-consuming and painstaking procedure.

A critical point which requires careful attention is to ensure that growth proceeds within the thermodynamic stability boundaries of the desired $\text{YBa}_2\text{Cu}_3\text{O}_{7-\delta}$ phase (the so-called 123-phase). The applicable stability principles have been investigated by Bormann and Nölting and Hammond and Bormann shown in Figure 2.6.

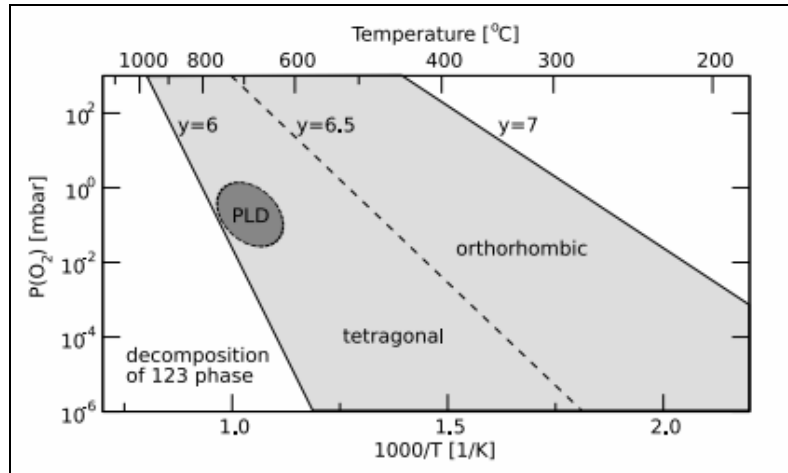


Figure 2.6. Temperature vs. partial oxygen pressure phase diagram for YBCO according to Bormann and Nölting and Hammond and Bormann. (Source: Schlepütz, 2009)

If the partial oxygen pressure during growth is lower than a certain critical pressure, the perovskite structure decomposes into various other phases like Y_2BaCuO_5 , BaCuO_2 and Cu_2O like many other deposition techniques as shown in Figure 2.5. This temperature-dependent phase boundary is located at the point where the oxygen content in the 123-phase drops below $y=6.0$, where $\delta > 1$, as shown in Figure 2.6. The stability regime is divided up into a tetragonal and an orthorhombic crystallographic phase. PLD, as most film growth techniques, obviously works optimally in the tetragonal phase just near the decomposition line. The phase transition from the tetragonal to the desired high- T_c orthorhombic 123-phase occurs for an oxygen content of at least 6.5 ($\delta \leq 0.50$). Seemingly, the best growth normally proceeds in the tetragonal phase close to the decomposition line, where the temperature, and hence the surface mobility, is high, and partial oxygen pressures, and therefore the oxygen reactivity, quite low. A transition to the orthorhombic phase and an ideal oxygenation of $7-\delta \approx 6.9$ of the compound is then achieved by in-situ post annealing step.

To help the oxygenation during growth and to avoid falling into the decomposition regime for the quite high substrate temperatures necessary to provide a good surface mobility for the desired two-dimensional growth of the films.

In this study we used single crystal MgO substrates, so we investigated the literature and focused on these parameters which selected MgO as a substrate during the deposition process. By the help of these parameters we tried to optimize our deposition system and to find out our suitable parameters. Table 2.1 shows some of these parameters taken from the literature.

Table 2.1. Typical parameters taken from the literature.

Sub. Type	Laser Fluence (J/cm ²)	Rep. Rate (Hz)	Ambient (mTorr)	Sub. Temp. (°C)	Target-Sub. Distance (cm)	Critical Temp. T _c (K)
LaAlO ₃	3.9	2	200 O ₂	800	3.5	88.3
LaAlO ₃	2.25	15	100-200 O ₂	808	-	91
LaAlO ₃	-	-	400 O ₂	720-800	50	-
SrTiO ₃	4	10	300 O ₂	780	5	89.5
MgO	1-2	8	250 O ₂	700	7	90
MgO	2	12.5	100 – 300 O ₂	700 -760	3.5 - 4.5	90
MgO	1.1 – 1.5	5	150	655- 810	-	92.5

2.5. Advantages and Disadvantages of PLD

Advantages of PLD technique can be summarized as indicated below;

- ❖ PLD provides stoichiometry transfer between target and substrate. It replicates the composition of target in the film.
- ❖ PLD uses laser as an energy source and it is located outside the chamber.
- ❖ In PLD, there are many adjustable parameters like laser fluence, target material, substrate type, deposition parameters, target to substrate geometry, etc.
- ❖ Pulsed nature of PLD means small spot size of the laser beam and small target size. This feature of PLD allows complex compounds and multilayer depositions.
- ❖ It is a fast deposition technique and by using PLD high quality samples can be grown in 10 or 15 minutes.
- ❖ Since it uses UHV during the process, it is a clean, low cost (one laser can serve many vacuum systems).
- ❖ During the process, PLD allows the usage of any ambient gas.
- ❖ PLD provides epitaxial thin films at low temperatures.
- ❖ In this technique both in-situ and ex-situ heat treatments are possible.
- ❖ PLD has high deposition rates, and this feature ensures decreasing impurities like oxygen contamination during deposition.
- ❖ PLD has a very wide application area in science and technology.

However, there are some disadvantages that causes detrimental effects on deposited films;

- ❖ Laser droplets; subsurface boiling, recoil ejection and exfoliation.
- ❖ Inhomogenous flux and angular energy distributions within the plume.
- ❖ Sometimes there are many macroscopic particulates that comes from plasma plume on the film surface.
- ❖ Crystallographic defects on the film caused by bombardment of high energetic ablation of particles.
- ❖ Mechanisms of PLD are difficult to explain and dependence on parameters are very difficult to control.

CHAPTER 3

EXPERIMENTAL

In this chapter, we will discuss the experimental details are given. In the first section, target preparation, briefly Lutetium, substrate cleaning is employed. In the next section, experimentally PLD, deposition parameters are discussed. In the final section, characterization techniques of the samples such as XRD, AFM, SEM and EDX are illustrated.

3.1. Lutetium Doped $\text{YBa}_2\text{Cu}_3\text{O}_{7-\delta}$ Target for PLD

3.1.1. Lutetium

Lutetium is a silvery white corrosion-resistant trivalent metal. It has the smallest atomic radius and is the heaviest and hardest of the rare earth elements like scandium, yttrium and fifteen lanthanides. It has the highest melting point (1652°C) between the lanthanides, and is difficult to find it in the pure form. Therefore, Lutetium is in the form of Lu_2O_3 . It tarnishes slowly in air, and burns easily at 150°C to form Lu_2O_3 .



Lutetium oxide has been attracting ever-growing attention from researchers for the last 15 years. This simple oxide doped with various lanthanides was fabricated and investigated in different forms such as nanocrystalline powders, thin films, sintered ceramics, single crystals.

Lutetium oxide is in the form of RE_2O_3 , and this type of oxides are called rare earth sesquioxides. These oxides are of interest in the science and technology of many applications such as high temperature materials. They can be used as precursors of high- T_c superconductors like $\text{REBa}_2\text{Cu}_3\text{O}_{7-\delta}$, generally indicated as the most promising materials for power applications of superconductivity due to their high critical current

density, J_c . Furthermore, Lu_2O_3 exhibits hygroscopic immunity compared to lanthanum oxide (La_2O_3).

In this study we selected Lutetium for doping into YBCO because Raychaudhuri et.al. reported that partial Lutetium substituted YBCO bulk samples shows much more Meissner effect than pure YBCO samples.

3.1.2. Target Preparation

The preparation of the targets to be used in the pulsed laser deposition of thin films is an important aspect of film growth because the target determines to a large extent, the stoichiometry, impurity content, laser energy coupling, particulate density, surface morphology, etc. of the film. Typically a target for PLD consists of a well compacted pellet, whose composition is identical to that of the desired film. Well sintered targets reduce particulate ejection during the ablation process. The target was prepared by the solid-state reaction method. The solid-state reaction method is a general method to produce HTSCs. The process consists of selection of raw materials, weighing, mixing, calcining and pulverizing steps. Figure 3.1 shows YBCO's flowchart and explains this common method.

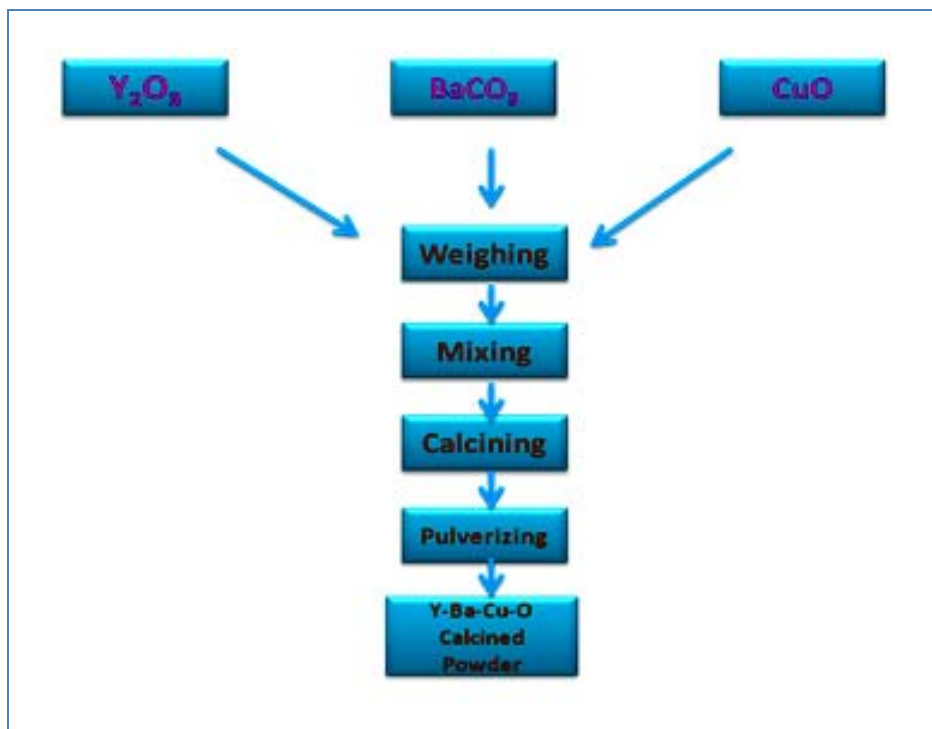


Figure 3.1. Flowchart of YBCO

In Lu doped YBCO target, powders of Y_2O_3 , $BaCO_3$, CuO and Lu_2O_3 combined in stoichiometric ratios, and they were mixed in an agate mortar for several hours to provide the uniformity and homogeneity of particle size. This mixture was calcined $920^\circ C$ for 24 h in air. After calcination, the mixture was crushed again and pressed into pellet. The pellet was sintered at $930^\circ C$ for 50h in air and cooled to room temperature at a cooling rate of $50^\circ C/min$. The weight of the target is about 8 gram and the area is about 3.96 cm^2 . Figure 3.2 displays the picture of our target. The ratios of the components in the reaction are,

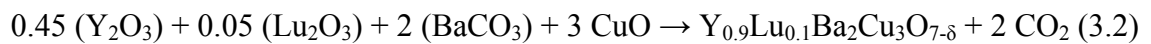


Figure 3.2. Lu doped YBCO target's diameters. The height is 0.26 cm.

3.2. Substrate Preparation and Cleaning

General requirements for an appropriate substrate material to produce the best quality epitaxial thin films are that chemical compatibility, lattice match, thermal expansion match, substrate surface quality, substrate homogeneity as mentioned in chapter one. An ideal substrate surface for superconducting thin film fabrication would be flat, uniform, dense and free of twins and other structural inhomogeneities. High- T_c YBCO superconducting thin films have been grown in a successful manner on a few materials such as Lanthanum Aluminate ($LaAlO_3$), Magnesium Oxide (MgO), Neodymium Gallate ($NdGaO_3$), Sapphire (Al_2O_3), Strontium Titanate ($SrTiO_3$), and Yttria stabilized Zirconium Oxide ($Y_2O_3-ZrO_3$). According to the knowledge of the

properties of these substrates, one can choose the ideal one for the designs depending on the application aim.

In this study, we used thin films deposited on $5 \times 5 \times 0.5 \text{ mm}^3$ single crystal MgO (100) substrates. The choice of MgO substrate is because MgO is an attractive substrate due to its low dielectric loss compared to better lattice matched substrates like LaAlO_3 , SrTiO_3 etc. It has the Rocksalt structure shown in Figure 3.3. This is a cubic structure with two interpenetrating FCC crystal lattices. This structure forms when the anion is larger than the cation. The close-packed direction of MgO lies along the (111) direction, which has the shortest distance between cations and anions. The properties of MgO is given in Table 3.1. MgO is also an easily available and inexpensive substrate. It also has a small thermal expansion mismatch with YBCO and is stable at the high processing temperatures required for growth. However, lattice constant of MgO is 4.21 \AA while that for YBCO is $a=3.82 \text{ \AA}$ and $b=3.89 \text{ \AA}$, giving a lattice mismatch of $\sim 10\%$. This is one of the reasons that the YBCO films contain several grain boundaries [Singh et al, 1988; Norton et al, 1989]. Furthermore, the quality of the films are found to be highly dependent on the surface preparation of MgO before growth [Moeckly et al, 1990]. Due to the sensitivity of the MgO surface to degradation, it is not possible to repeatedly grow high quality YBCO films on used MgO substrates.

Table 3.1. Typical properties of single crystal MgO substrates.

<i>Substrate</i>	<i>MgO</i>
Crystal Structure	Cubic
Lattice Parameter	$a = 4.216$
Thermal Conductivity ($\text{WK}^{-1}\text{cm}^{-1}$)	3
Specific Heat ($\text{JK}^{-1}\text{cm}^{-3}$)	0.53
Melting Point ($^{\circ}\text{C}$)	2800

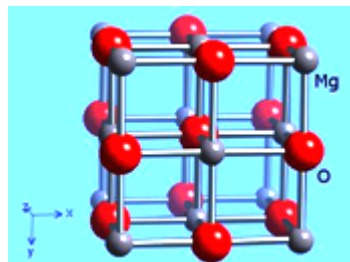


Figure 3.3. Crystal structure of magnesium oxide
(Source: webelements 2010)

Substrate cleaning is a very important step for the process of film deposition. Even a small dust particle on the substrate surface might inhibit the formation of a uniform film structure. Consequently, substrates have to clean as good as possible before the deposition process. For the purpose of cleaning our MgO substrates the following steps must be performed:

- ❖ Cleaning MgO substrates ultrasonically in acetone for 1 hour.
- ❖ In the following, cleaning substrates ultrasonically in alcohol for 1 hour.
- ❖ In the end, drying them with N₂ gas flow.

The MgO surfaces are hygroscopic and is easily degraded by humid environment, and as a result of that the formation of hydroxides of Mg occurs. Hence, special care has to be taken to avoid such degradation and contamination of the substrate surfaces, and all the substrates are stored in vacuum dessicators.

3.3. Experimental Aspects of PLD

Pulsed laser deposition of Lu doped YBCO thin films on MgO substrates were achieved in our laboratory by using a commercially obtained system from the Neocera Corporation. Our system includes an excimer laser with a KrF radiation that has a wavelength of 248 nm and pulse duration of 18 ns, a toxic gas cabinet for the containment of the lasing gases, an 18-inch diameter spherical deposition chamber with pumping stack, and the connected laser optics. In the following sections, the properties of our system will be discussed.

3.3.1. Laser and Laser Optics

As mentioned above, the laser is a KrF excimer laser of wavelength 248 nm and pulse width of 18 ns. The maximum output energy of the laser is 125 mJ at an operating voltage of 16 kV. Although the pulse repetition rate can be varied in the range of 1 to 20 Hz, we used 3 to 8 Hz to deposit our films onto the substrates. The laser optics used to focus the laser pulse onto the target consists of a mirror which is used to

guide the laser, and lens to focus the laser beam. The beam is focused onto the target at 45° by the help of the lens. All these equipments are made up of UV graded fused silica. The mirrors have a coating that provides the reflection at 45°. Due to the lens dimension, same as the beam, small misalignment of the mirror causes about 32 % laser power loss before reaching the target. Figure 3.4 exhibits the optical system of our PLD system.

A combination of the high absorption of the 248 nm UV laser beam by YBCO and the low thermal conductivity creates dielectric breakdown in the YBCO and instantaneously high absorption in a very thin surface layer of the target material. The name excimer comes from “excited dimer”. An excited dimer is a diatomic molecule in an excited state. During the laser operation the creation of the excited KrF molecule proceeds with the following reaction:



Here the Ne atoms serve as a collision partner, without which the reaction cannot proceed to form the KrF excimer.

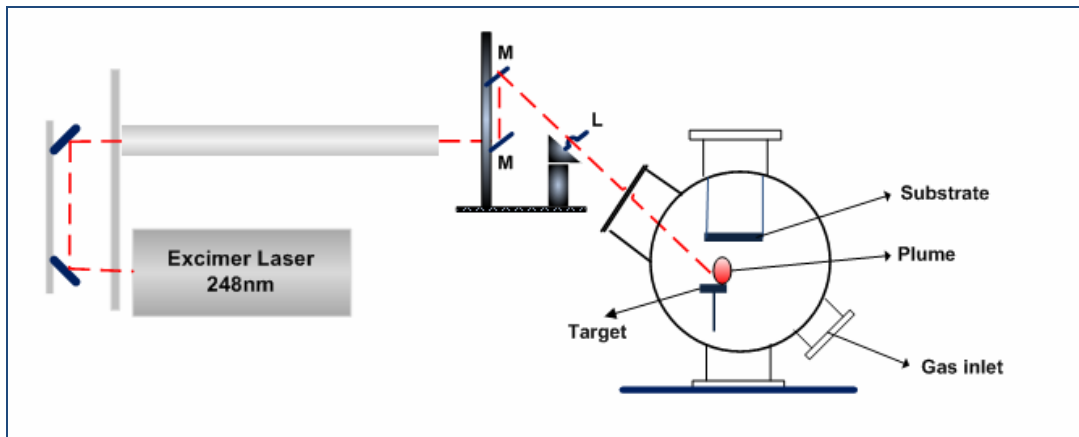


Figure 3.4. The optic system and the vacuum chamber of PLD.

3.3.2. Deposition Chamber and Pumping

The deposition chamber is an 18-inch stainless steel (SS) chamber with a number of ports serving the functions of viewing, laser window, vacuum gauges etc.

Multi-target holder which can hold up to 6 targets, shown in Figure 3.7 and substrate holder are inserted inside the chamber without breaking the vacuum. The substrates are attached with the surface parallel to the target surface at a target-to-substrate distance of almost 2 to 10 cm. We used the distance of about 5 to 7,5 cm during the process. Inside of the deposition chamber in our lab is shown in Figure 3.6. During the deposition, the target is spinned around its axis and also rastered with the angles $\pm 15^\circ$ around the carousel target axis to maximize useful target area and prevent the target burn out. Also the substrate holder rotates to increase the uniformity of the film during deposition. In addition, the deposition process can be performed both manually and automatically by the software.

The substrate heater that is above the substrate holder is designed to reach the temperature value of around 900 °C, and a shutter provides the necessary protection during the ablation of the target which is known as pre-ablation.

Due to the relatively high deposition rate, base pressure in the range 10^{-7} torr is adequate for PLD. This pressure range, which is in the high vacuum (HV) regime, is necessary for the film growth to reduce surface contamination. To achieve this, turbo-molecular pump is a good choice because it avoids hydrocarbon contamination and allows for the fast evacuation of the deposition chamber. The turbo-molecular pump and scroll pump as a backing pump are connected at the bottom of the chamber. The chamber is vented with nitrogen gas each time a substrate or a target has to be inserted, than the evacuation begins from the ambient pressure. Therefore, a valve system allows a direct connection of the chamber with the backing pump. When the humidity level in the chamber increased too much and breaks the vacuum, the chamber is baked from outside with the help of heating tapes. A special care has to be taken for the temperature not to reach 100 °C.

A gate valve separates the chamber from the turbo-molecular pump, and it controls the speed by changing the area of the aperture connecting the chamber and the pump. An ambient gas oxygen for YBCO deposition is introduced in the chamber, and

pressure is adjusted to the desired value in the range of 1 mtorr to 1 torr using a flux meter and a needle valve; and the pressure is measured by ionization vacuum gauge.

In Figure 3.5 six target carousel for in-site multilayer depositions, in Figure 3.6 the PLD system in our laboratory at İYTE Physics department and in Figure 3.7 interior of the deposition chamber are illustrated.



Figure 3.5. A Neocera six target carousel for in-situ multilayer depositions.

(Source: neocera 2011)

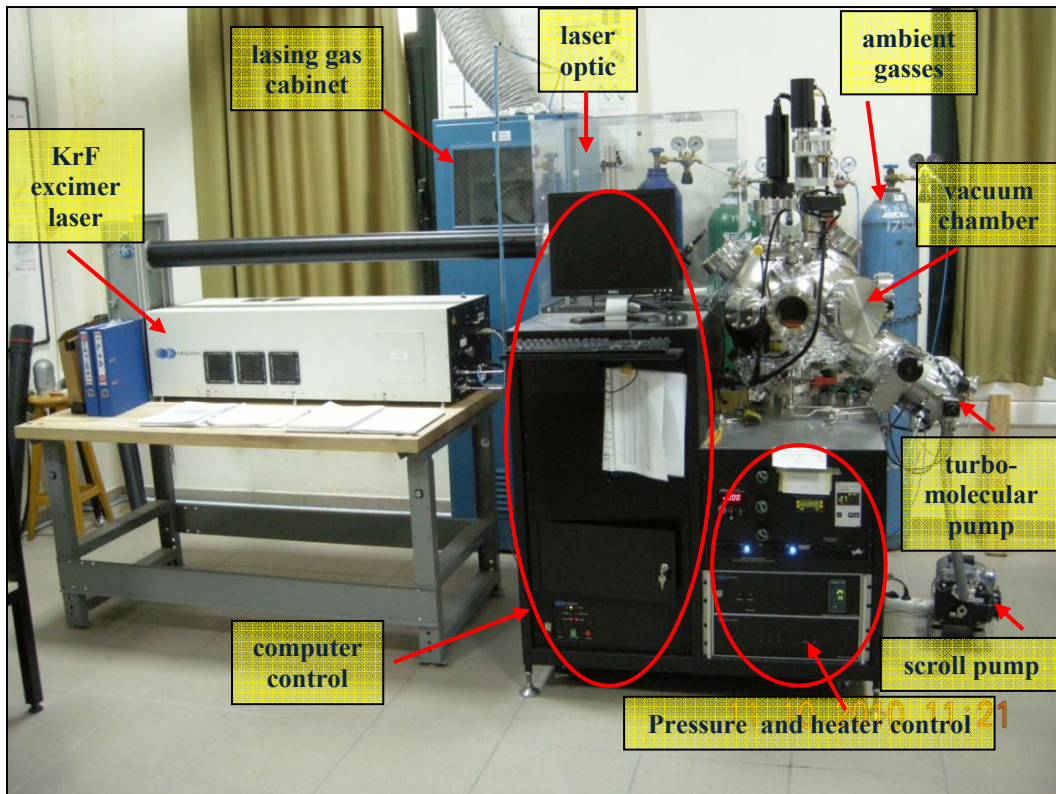


Figure 3.6. PLD in our lab.

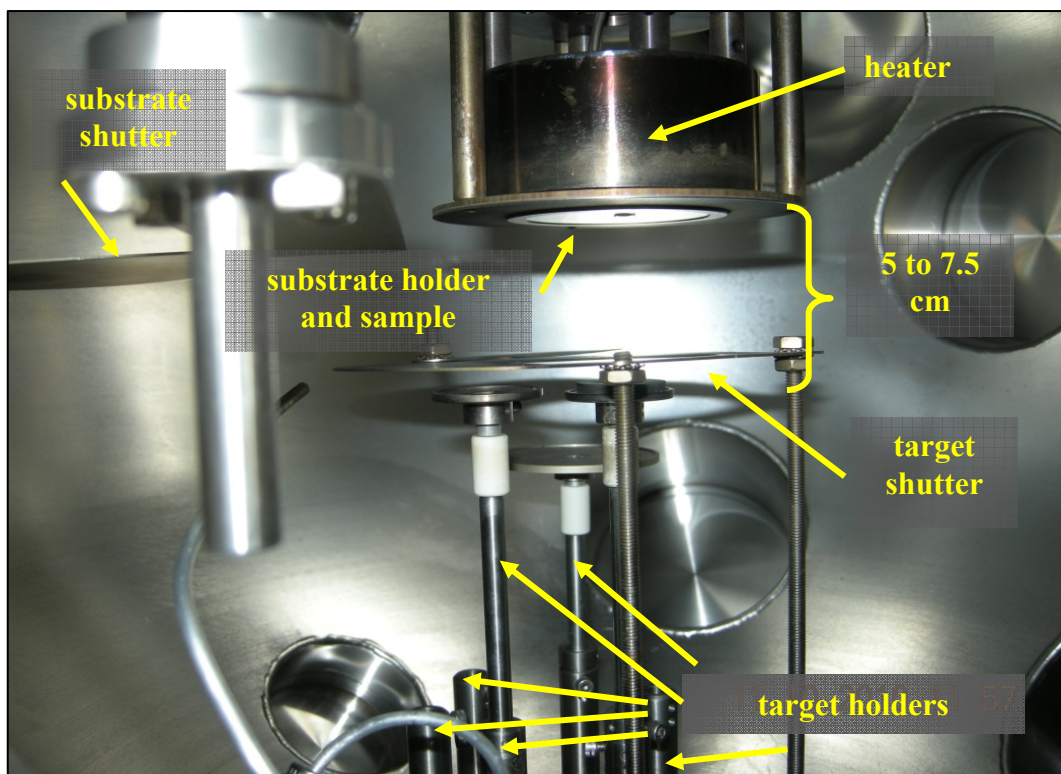


Figure 3.7. Target and substrate holders. Target and substrate shutters.

3.3.3. Deposition Parameters

The $Y_{0.9}Lu_{0.1}Ba_2Cu_2O_{7-\delta}$ target was sanded down to fresh uniform surface with Water Proof Silicon Carbide Supraflex paper P1000A sandpaper. The target surface was cleaned off with acetone and alcohol, and dried with N_2 gas flow. The substrate holder plate was cleaned with diluted HCl solution to remove the materials come from the previous deposition. Afterwards, the plate was polished with the same quality sandpaper (P1000A) to remove waste silver paint and cleaned with acetone, alcohol and DI water. 5x5x0.5mm, (100) MgO substrate was taken from the vacuum dessicator and mounted on the holder plate with silver paint, from SPI Inc. The substrate holder then baked at about 100 °C for 5 minutes to dry up the silver paint before loading the holder inside the chamber. After the target and the substrate holder were loaded into the chamber, the system was vacuumed down to 10^{-7} torr in about 6 hours. The MgO substrate was brought to the temperature 800°C at a ramp rate of 40°C per minute. In this temperature value the substrate was annealed for 30 minutes in 10^{-7} torr vacuum. During this annealing the 248 nm excimer laser warmed up for the operation and turbo-molecular pump slowed down from 833 Hz speed to 190 Hz. Once these were completed, oxygen as an ambient gas was introduced into the chamber the pressure range of ~300 mtorr. The target and the substrate rotated at a constant velocity to obtain a uniform film surface and to avoid the target burn out. The substrate holder spinned with 25 degree per second, the target rotates at 40 degree per second and rastered from -15° to 15° with a speed of 10 degree per second during the whole process. The laser power was set to 14 kV before preablation. The target was preablated with 900 laser pulses at 5 Hz to have fresh surface with substrate shutter was closed. After the preablation, the substrate shutter was opened and deposition run with 15000 laser shots at 3 Hz in 300 mtorr oxygen atmosphere. The laser energy density during preablation was 1,97 J/cm² and laser spot size area was 2 mm². After the deposition process, the temperature decreased to 650°C with a speed of 5° per minute and the pressure was slowly increased at the same time. At 7 torr O₂ pressure, the turbo pump was stopped to quickly increase the pressure. The substrate was annealed at 500°C temperature for 30 minutes and at the same time 250 to 300 torr O₂ pressure. Lastly, the system was cooled down to room temperature. The film was demonstrated ~240 Ω resistance at room temperature. In

Figure 3.8 the position of the substrate on the holder is shown, and in Figure 3.9 the deposition parameters are illustrated.

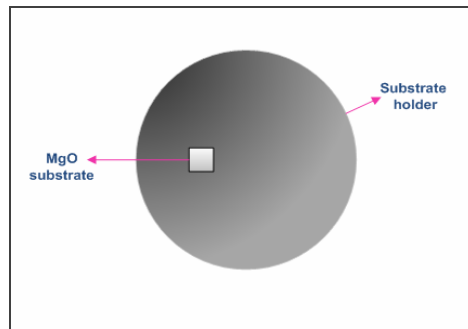


Figure 3.8. Schematic illustration of the substrate on holder.

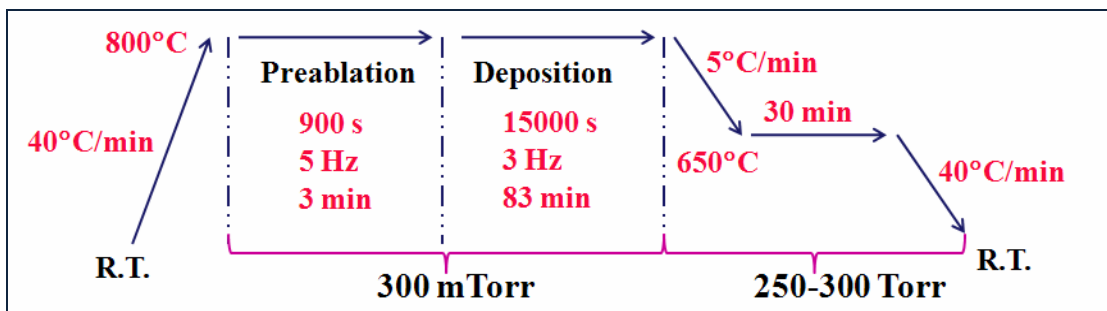


Figure 3.9. Deposition parameters

Before we obtain our optimized parameters for pulsed laser deposition process above, we tried to many different parameters for this purpose. In Table 3.1 there are some of our old parameters and successful ones are given. During deposition, the shape of the plume as a picture is illustrated in Figure 3.10.



Figure 3.10. The image of the plume during deposition

Table 3.2 Some of our tested deposition parameters and the ones in rectangle are successful ones.

Sub. Type	Laser Fluence (J/cm ²)	Laser Energy (kV)	Rep. Rate (Hz)	Ambient (mTorr)	Sub. Temp. (°C)	Target-Sub. Distance (cm)	Deposition Time (min)	Annealing Temp. (°C)	Annealing Time (min) and Pressure (Torr)
MgO	3.2	15	5	300 O ₂	780	3	30 (9000s)	500	300 Torr-1 h
MgO	2.25	15	6	100-200 O ₂	800	4.5	45 (16500s)	580	250 Torr-50 min
MgO	3	14	8	400 O ₂	720-800	50	20 (9600s)	620	150 Torr-45 min
MgO	2.1	14	10	300 O ₂	780	5	30 (18000)	600	350 Torr-30 min
MgO	2.5	12	2	150 O ₂	780	7	100 (12000s)	550	750 Torr-1 h
MgO	3.5	16	4	250 O ₂	760	6.5	33.3 (8000s)	550	650 Torr-30 min.
MgO	1.5	12	3	150 O ₂	790	6	55 (9900s)	530	500 Torr-30 min
MgO	3.22	14	5	300 O ₂	800	6.5	50 min (15000s)	650	250 Torr-45 min
MgO	3	14	3	300 O ₂	800	7	83 min (15000 s)	670	300 Torr-30 min

3.4. Characterization Techniques

3.4.1. Electrical Characterization

3.4.1.1. Resistance vs Temperature Measurements

3.4.1.1.1. Cryogenics

The title high temperature superconductors refers to a class of materials with high transition temperatures relative to the superconducting materials. To achieve superconducting behavior, one must cool the sample significantly below room temperature. Such cooling may be achieved by using a mechanical cooling system such as refrigerator or by direct cooling with cold liquids, known as cryogens.

Simple closed-cycle refrigerators can produce temperatures down to about 4K and provide an easy way of performing low-temperature measurements. The disadvantage of most refrigerators is that the geometry of their construction, which is necessary for the cooling operation, is not well suited to many of the different types of

measurements performed. For this reason, most experiments on high temperature superconductors are made using cryogenic liquids.

The most common cryogens used are liquid nitrogen (has a boiling point of 77 K) and liquid helium (which boils at 4.2 K). Since the transition temperatures of the high- T_c materials are often above 77 K, liquid nitrogen may provide sufficiently low temperatures for many experiments. However, for measurements on samples with lower transition temperatures or at high magnetic fields, it will be necessary to use liquid helium for cooling samples.

In our lab we use helium gas flow cryostat system, in which the sample is heated or cooled by flowing helium vapor. For measurements between about 4 K and room temperature, liquid helium from a reservoir flows through a needle valve and capillary tube to a resistive heater. It then flows vertically up through the sample space and out to atmosphere through a flow valve. The temperature of the vapor, and thus the sample, is controlled by the heater. A thermometer at the heater allows the vapor temperature to be monitored, and by connecting to a controller, temperature of the following vapor may be monitored. To operate at lower temperatures down to 1.4 K, liquid helium is allowed through the capillary tube into the sample space, where it is pumped to produce evaporative cooling.

3.4.1.1.2. Electrical Contacts

For electrical transport measurements, it is important to maintain low contact resistance so that there is little dissipation in the contacts. Attaching measurement leads to high- T_c superconductors has been problematic because of the poor quality of sample surface layers. Several different techniques have been used to achieve low-resistance electrical contacts to both single crystals and thin films. The simplest method involves direct contact of the measurement wire to the surface of the sample. This may be done using an electrically conductive silver paint which binds the wire to the surface. This technique is usually known as four-point contact and we used this method for our R-T measurements. Figure 3.11 displays the R-T measurement system built in our laboratory.

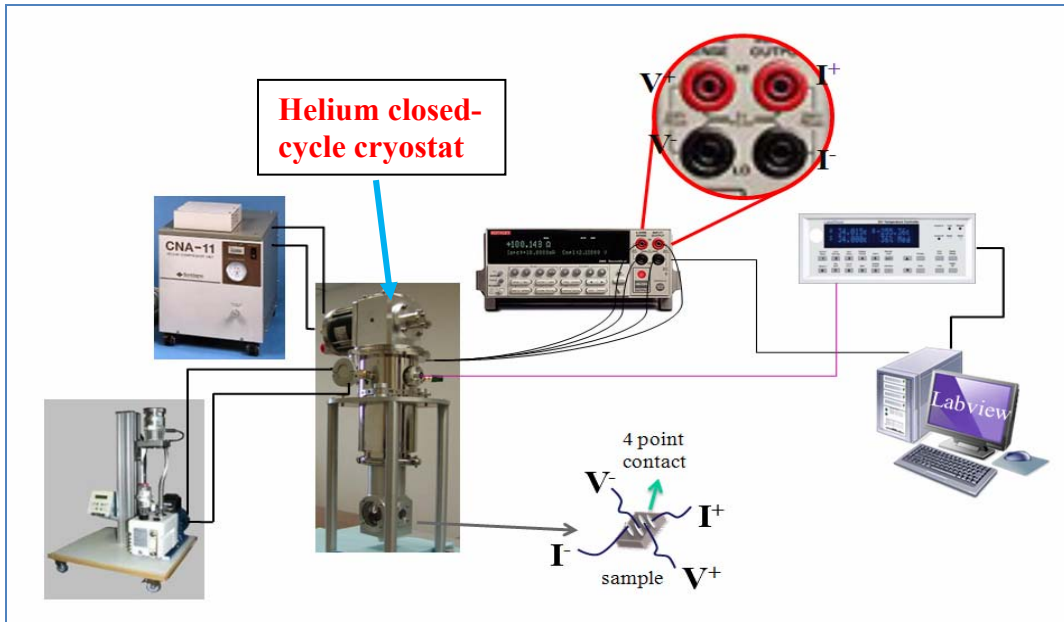


Figure 3.11. R-T characterization setup in our lab

3.4.2. Surface Characterization

$Y_{0.9}Lu_{0.1}Ba_2Cu_2O_{7-\delta}$ thin films were characterized by structural, morphological, compositional and electrical analyses. The structural analysis is carried out by X-Ray Diffraction (XRD). The Scanning Electron Microscopy (SEM) and Atomic Force Microscopy (AFM) gives information on the surface morphology and the Energy Dispersive X-ray analysis (EDX) individuates the chemical composition on the surface of our films.

3.4.2.1. X-Ray Diffraction (XRD)

X-ray diffraction is a powerful, fast and nondestructive method of determining crystal structure, phase, grain size, strain and grain orientation in materials. Diffraction is a scattering mechanism where x-rays scattered by large numbers of periodically arranged atoms in a lattice create phase relations. X-ray diffraction phenomenon follows Bragg's Law for diffraction which describes the condition for constructive interference for X-rays scattering from atomic planes of a crystal. The condition for constructive interference is,

$$n\lambda = 2d\sin\theta \quad (3.1)$$

Here θ is the angle of incidence relative to the planes, n is an integer and λ is the wavelength of the x-ray. In Figure 3.12 the diffraction geometry of the x-rays is shown. The Bragg's Law requires that θ and λ be matched for diffraction. By changing λ or the orientation of a single crystal, this condition should be done. When x-rays are incident under a very small angle with the sample surface, the technique is often called grazing incidence x-ray analysis (GIXA) and it is useful for thin film analysis. Film thickness and roughness can be analyzed with GIXA because the reflection of the beam occurs at interfaces.

The θ - 2θ XRD measurements of the films were made by using a Philips X'Pert Pro X-ray diffractometer with Cu- K_{α} $\lambda=1.5418 \text{ \AA}$. The samples were detected with the angles between 5 to 80 degrees.

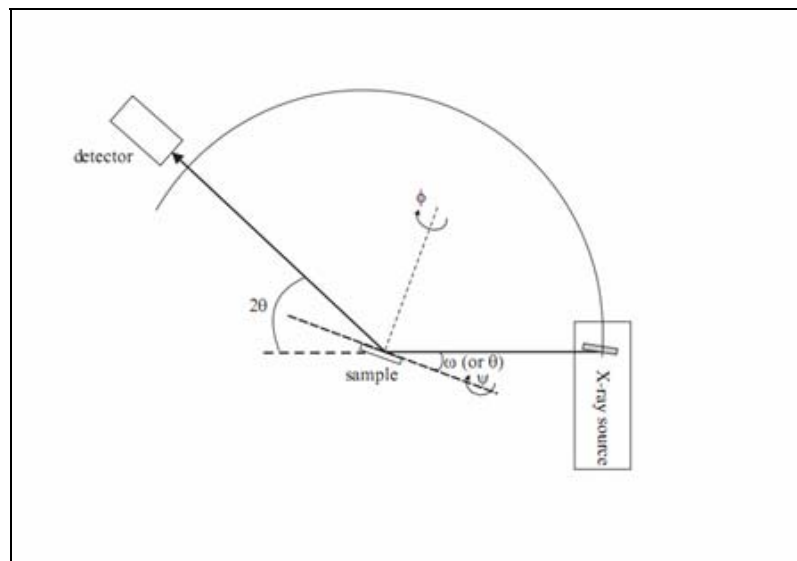


Figure 3.12. 2θ X-ray diffraction geometry for phase, composition and normal-to-substrate texture measurements. (Source: Malisa, 2005)

3.4.2.2. Atomic Force Microscopy (AFM)

Atomic Force Microscopy is a useful method for the topography and structural study of epitaxial thin films. AFM is based on the detection of a low power laser beam reflected by the edge of a soft cantilever. A typical cantilever for the system is made up of silicon tip material and oscillates freely in air at its resonant frequency. AFM consists

of two operating modes are tapping (non-contact) mode and contact mode. In the tapping mode, the tip does not touch the sample surface, but in the contact mode there is an interaction between the tip and the substrate surface. This causes the removal of the atoms from their places on the surface, and this leads to damages on the film surface. Eventually, the tapping mode gives better image results compared to contact mode. In Figure 3.13 a typical AFM is illustrated below.

In this study, AFM images were taken from a Multimode SPM, Nanoscope IV Digital Instrument. This analysis gave information about our film surfaces.

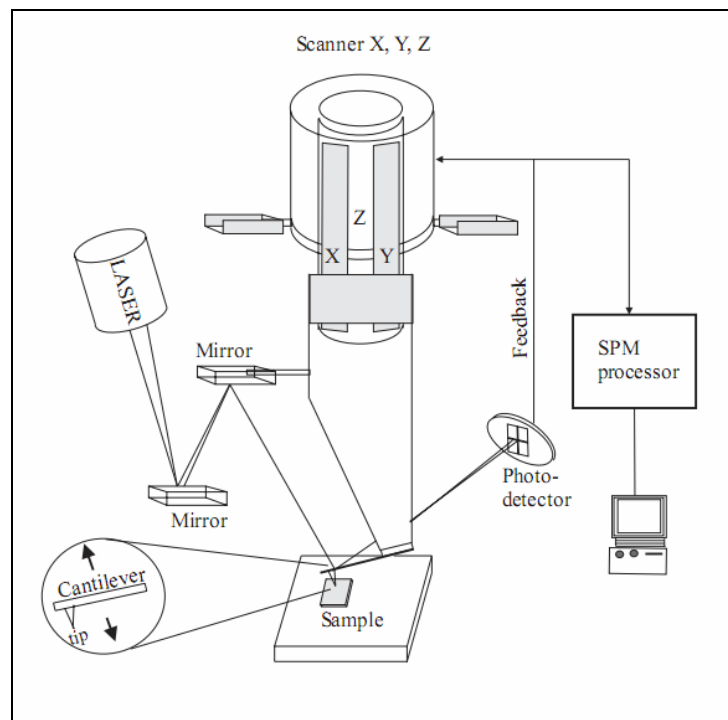


Figure 3.13. A schematic diagram of an atomic force microscope (AFM).

(Source: Malisa, 2005)

3.4.2.3. Scanning Electron Microscopy (SEM) and Energy Dispersive X-ray Spectroscopy (EDX or EDS)

Scanning electron microscopy is a typical method used for characterization of the surface morphology of the thin films. SEM is a very beneficial technique for a quick view of the whole area of the surface of a given film. Compared to other techniques like AFM, SEM is a very quick method for surface characterization. From the point of working principle, SEM depends on sending highly focused electrons on the sample, in

order to scan its surface in vacuum. The generated secondary electrons are accelerated toward a detector. The pictures formed to provide information down to less than a micron size.

Energy dispersive x-ray spectroscopy, EDX or EDS, is a chemical microanalysis technique performed in conjunction with a scanning electron microscope. In this technique, an electron beam of 10-20 keV hits the surface a conducting sample that causes x-rays to be emitted from the point of incidence. The x-ray detector measures the number of emitted x-rays according to their energy. By collecting and analyzing the energy of these x-rays, the component elements of the sample can be determined. From the EDX spectrum we can easily identified the elements Lu, Y, Ba, Cu, O and Mg in our samples.

In this study, SEM (Phillips XL-30S FEG) was used to analyze the surface of the films grown on MgO substrates.

CHAPTER 4

RESULTS AND DISCUSSION

In this chapter, experimental results are mentioned. Structural characterization of the Lu doped YBCO thin films deposited by pulsed laser deposition are performed and their results are presented. Electrical characterization is performed by showing R-T measurement graphs.

4.1. Structural Characterization

In this section, XRD results of both the film and the target and EDX result of the target are illustrated, AFM and SEM results of the film are presented. The Lu doped $\text{YBa}_2\text{Cu}_3\text{O}_{7-\delta}$ thin films of about 400 to 500 nm thickness were grown on single crystal ($5 \times 5 \times 0.5 \text{ mm}^3$)- sized MgO (100) substrates by pulsed laser deposition. The films were characterized by structural, morphological, compositional and electrical analysis. Structural analysis is performed by X-Ray Diffraction (XRD) from which the information on the phases and their crystallographic orientation with respect to the substrate can be obtained. The Scanning Electron Microscope (SEM) and Atomic Force Microscope (AFM) give information on the film morphology and the Energy Dispersive X-ray analysis (EDX) differentiates the chemical species analyzing the x-rays emitted from the samples when they are hit by the SEM electron beam.

4.1.1. XRD Results

XRD patterns of both Lu doped YBCO target used in PLD during deposition and Lu doped YBCO thin film at optimized growth parameters are displayed in Figure 4.1 and 4.2. According to Philips X'Pert Pro X-ray diffractometer's data analyse program, the Lutetium peaks begin from 29 and end with 75 in 2Θ degrees of Lu doped YBCO target. These peaks continue with intervals from 29 to 75. In our study the

Lutetium doping level is quite low as mentioned before and the XRD peaks of Lutetium is spread through these values which are in ovals.

The YBCO peaks are easily noticed from the XRD result of Lu doped YBCO thin film in Figure 4.2 as the same in the literature. The same peaks at the same 2θ values lie in the literature but there might be some oxygenation problem during the PLD process because the other peaks that come after (007) peak can't be displayed.

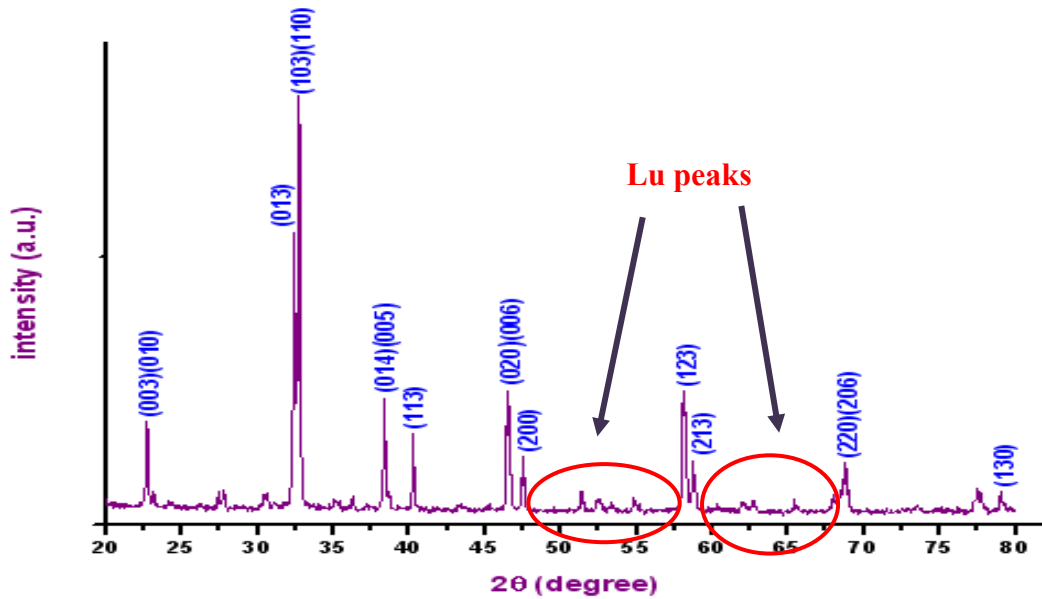


Figure 4.1. XRD result of Lu doped YBCO target

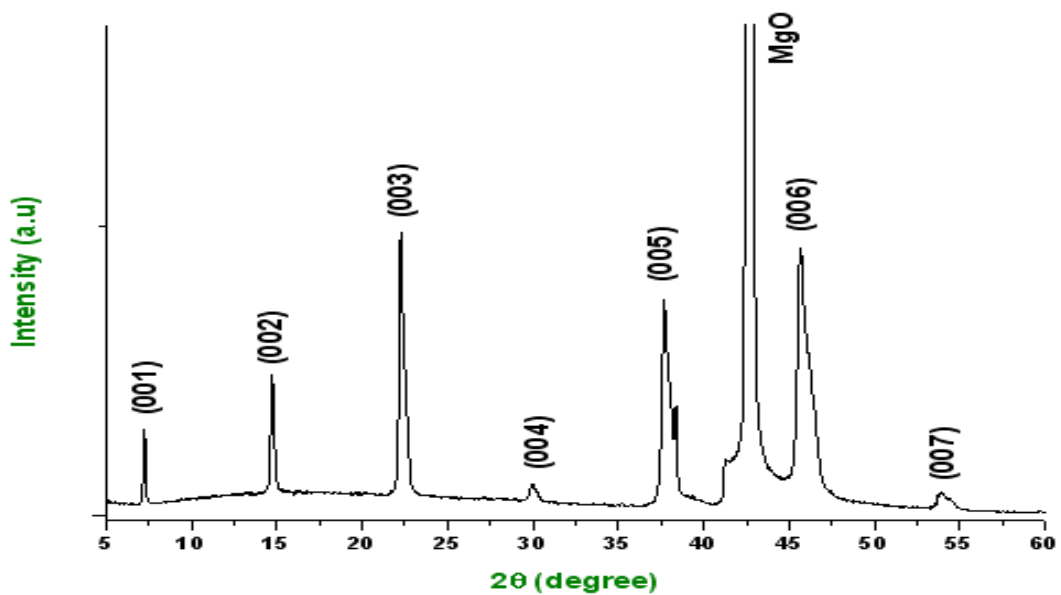


Figure 4.2. XRD result of Lu doped YBCO thin film on MgO substrate.

4.1.2. SEM and EDX Results

Figure 4.3 shows the EDX result of our Lu doped YBCO target. By using EDX analysis we found out the elements Lu, Ba, Cu, O and Mg which are in the target composition. As you see from the Figure 4.3, the Lutetium amount is very low. There is some carbon arises from this analysis and that might belong to impurities inside our bulk target.

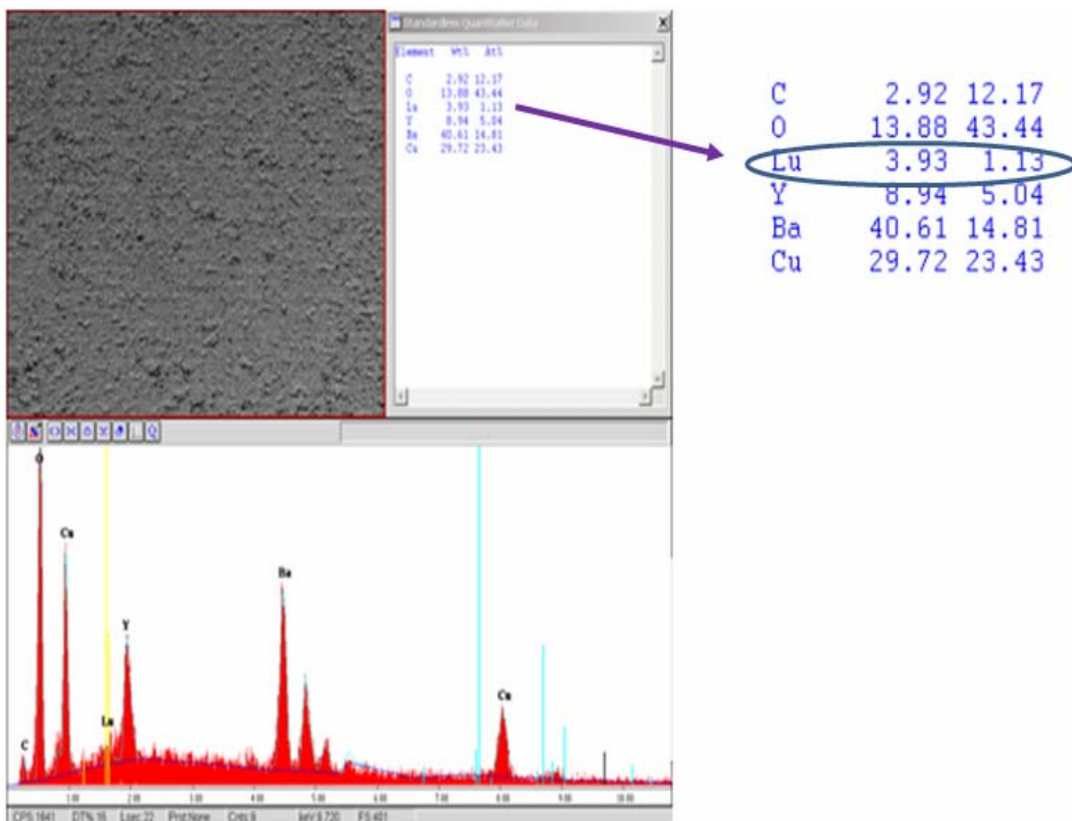


Figure 4.3 EDX result of Lutetium doped YBCO target

From the literature, the changes in the deposition temperature causes changes in the film quality. Low temperatures produces poorly ordered films. Figure 4.4 shows the Lu doped YBCO film deposited at 800 °C, with an oxygen partial pressure of 300 mTorr, and laser power of 14 kV, and in-situ annealing temperature of 650 °C for 45 minutes.

One of the largest factors, which can affect the overall smoothness of the specimen is the production of laser droplets. These particulates are produced by collisions of ions within the plume before they react with the surface. The material with

droplets often does not have enough energy to recrystallize as the correct stoichiometry, $\text{YBa}_2\text{Cu}_3\text{O}_{7-\delta}$, once reaching the substrate. Laser droplets typically yield nonconducting particulate matter that disrupt further deposition of the desired material within that region of the deposited film. To quantified the density of laser droplets, the films are examined by scanning electron microscope. Several pictures are taken at specified magnifications and the areas of these droplets range from 600nm to 4 μm .

In Figure 4.4A, the film morphology is examined as well. There are a large number of laser droplets seem as round white spots marking the surface of the film. Looking at a higher magnification, Figure 4.4B, shows the outgrowth of elongated rectangular grains evocative of a-axis films on top of the smooth coalesced background typical of c-axis film. As the surface of the film becomes further removed from the substrate, the effective temperature of the surface drops with deposition. It can be inferred from this information that an a-axis overlayer can grow atop the c-axis oriented film when the deposition temperature is close to the boundary for c-axis deposition, which appears to be the case for these samples.

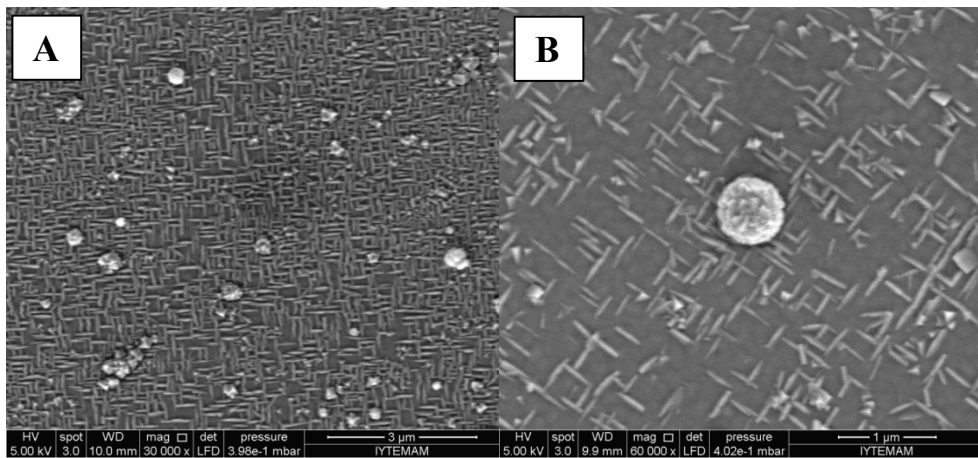


Figure 4.4. SEM for the films deposited at 800 °C, 300 mTorr, and 14 kV. Image A reveals several round white spots, which are identified as laser droplets. Image B shows an a-axis growing as a “basket-wave pattern”, indicative of a-axis orientation, on the mosaic pattern indicative of c-axis films. Image A has 30,000 and image B has 60,000 magnifications.

The films shown in Figure 4.5 was deposited at the same parameters but different in-situ annealing temperature, and delay time. These films were annealed at 670 °C for 30 minutes.

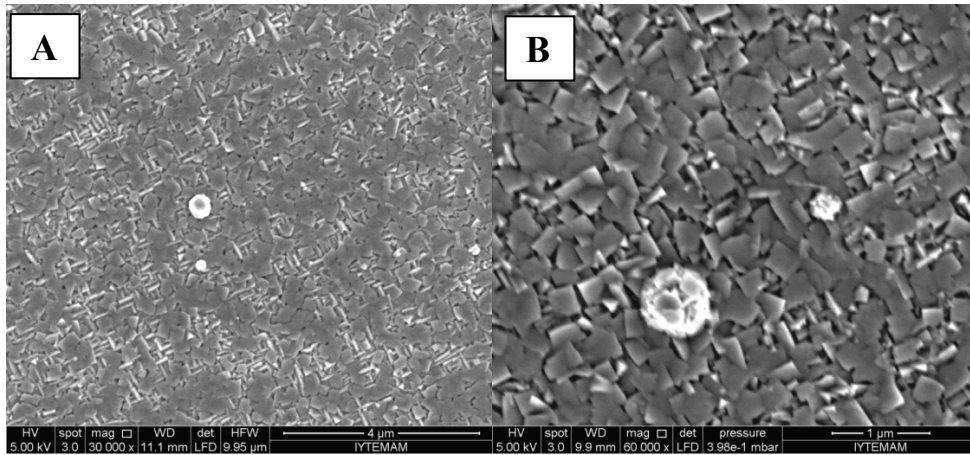


Figure 4.5 Lu doped YBCO films had the same deposition parameters but these films were annealed at 670 °C for 30 minutes. The disorder seen on Figure 4.4 is also seen in the image A. As is shown in image B, the round spots are laser droplets that are imbedded in the film. Image A has 30,000 and image B has 60,000 magnifications. In addition to the disorder caused by these spots, the mosaic square structure seen in high quality c-axis films does not match perfectly.

The cause for the disorder is easier to see when examining the film using SEM. There are a large number of laser droplets plainly visible. Unlike Figure 4.4A, these droplets have larger sizes and more rounded shapes seeming to indicate that the 300 mTorr oxygen partial pressure may not be high enough to sharpen the plume sufficiently.

4.1.3. AFM Results

The AFM images were also taken to provide a clear insight into the surface morphology of the Lu doped YBCO films. In Figure 4.6 the AFM photos of our samples are shown. In Figure 4.6A the mean surface roughness, R_a , of the Lu doped YBCO thin films grown on MgO substrates within scanned area of $4.331 \mu\text{m}^2$ was measured as about 6.597 nm, and besides this image its 3-dimensional graph is illustrated to see how rough the film surface was. In Figure 4.6B the R_a value with a scanned area of $4.076 \mu\text{m}^2$ was measured 7.627 nm. Besides this image its 3-D version is placed.

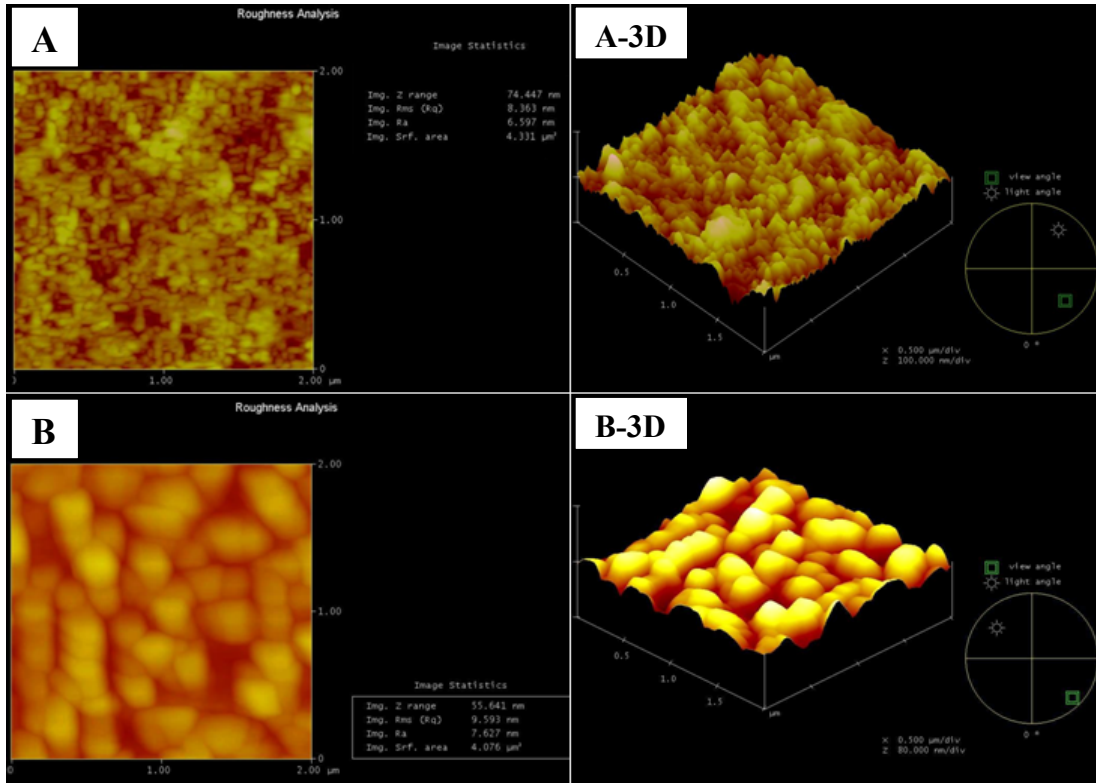


Figure 4.6. AFM surface roughness analysis of the Lu doped YBCO thin film on MgO substrates.

4.2. Electrical Characterization of Lu Doped YBCO Thin Films

4.2.1. Resistance vs Temperature Measurements

Another technique used to quantify the quality of the film is measuring its resistance versus temperature characteristics. A normal metal often has a linear response of resistance with temperature. A superconductor undergoes a deviation from this at its superconducting temperature. According to the literature, this transition for YBCO should occur at $\approx 92\text{K}$. However, inefficient coupling between adjacent grains, the inclusion of impurity phases, or the loss of oxygen from the lattice can cause both a drop in this temperature and a broadening of the transition region.

In this study we found out two useful parameters as mentioned in chapter 3. These parameters were shown in Table 3.1 and the in-situ annealing processes is very important for the growth films to have higher transition temperatures. One of these parameters was; the samples were kept at $650\text{ }^\circ\text{C}$ temperature, 250 Torr O_2 pressure for 45 minutes and the other was; the samples were kept at $670\text{ }^\circ\text{C}$, 300 Torr O_2 pressure for

30 minutes. In Figure 4.7 and Figure 4.8 the R-T measurements of these two parameters are illustrated. According to annealing time in O₂ pressure and annealing temperature, the transition temperature changes. The samples have shown a sharp transition at temperatures nearly 82 K and 83.5 K.

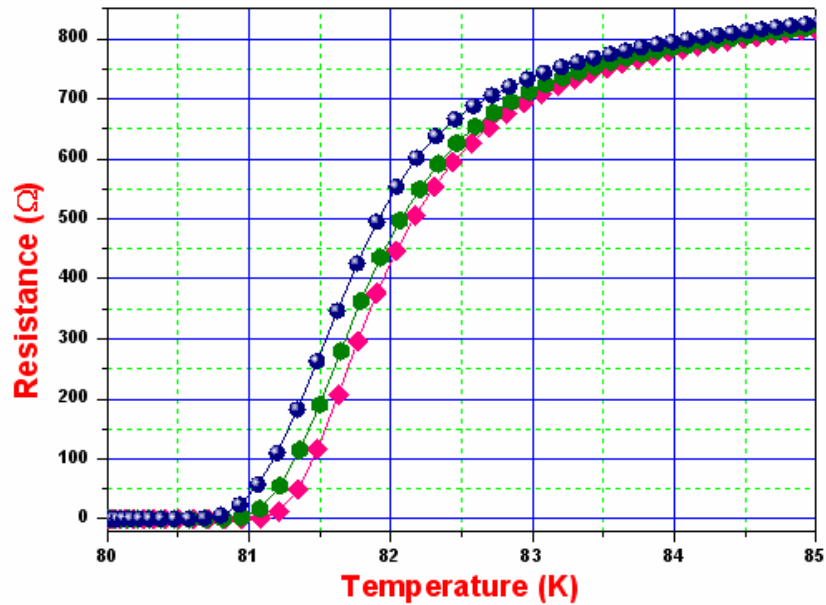


Figure 4.7. R-T measurement of the films that produced using (670 °C, 300 Torr O₂ pressure, 30 min.) annealing process.

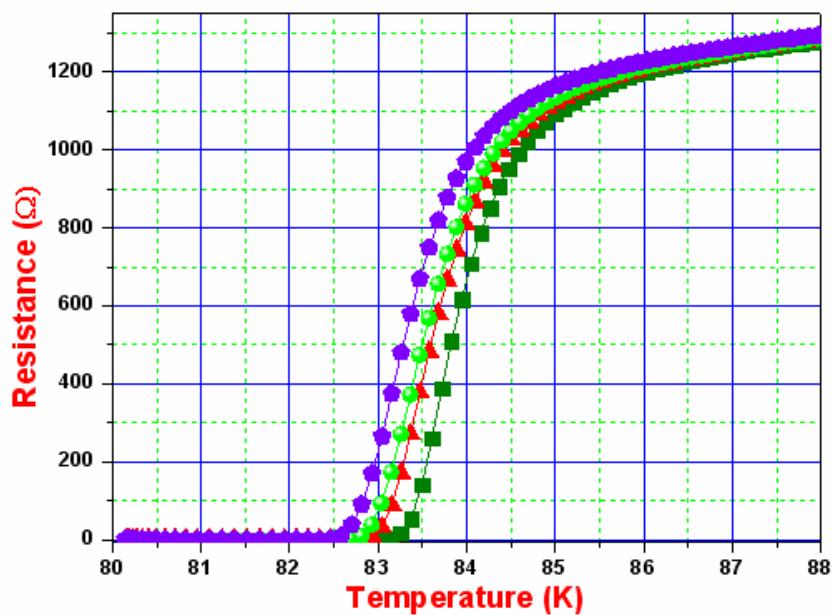


Figure 4.8. R-T measurement of the films that produced using (650 °C, 250 Torr O₂ pressure, 45 min.) annealing process.

CHAPTER 5

CONCLUSIONS

Presently high temperature superconductor thin films for electronic applications are dominated by $\text{YBa}_2\text{Cu}_3\text{O}_{7-\delta}$ and related 123 materials. These materials are one of the most complicated materials subjected to technological development today. Growth of epitaxial, complex oxide thin films poses a particular challenge because of the incompatibility of chemical reactivity and the varying volatility of the elements involved. Pulsed laser deposition, shortly PLD, is one of the most convenient methods to obtain thin films of these materials. During PLD tiny amounts of vaporized material originated from superconducting bulk target are deposited on a substrate in a controlled environment and deposition regime. It is done in such a way that the original stoichiometry of the bulk material is preserved and high quality superconducting thin films can be performed.

In this study, we fabricated Lutetium doped YBCO thin films on MgO substrates by using pulsed laser deposition technique. For this aim, we firstly prepared a Lutetium doped YBCO target by using solid-state reaction method from commercially available Y_2O_3 , BaCO_3 , CuO and Lu_2O_3 materials. Lutetium oxide is in the form of RE_2O_3 as mentioned in chapter 3, and they are called rare earth sesquioxides. These oxides are of interest in the science and technology in many applications. They can be used as precursors of high temperature superconductors like $\text{REBa}_2\text{Cu}_3\text{O}_{7-\delta}$. Secondly, (100) single crystal MgO substrates were selected to use during this study. Afterwords, by using PLD system and in-situ annealing process we tried to obtain epitaxially grown Lu doped YBCO thin films. For this purpose, lots of different PLD parameters such as, laser fluence, laser energy, laser repetition rate, oxygen pressure, substrate temperature, annealing time and annealing temperature were adjusted during the process. This is named as PLD optimization in literature and it took to much time to obtain the right parameters for our deposition system. We found out that to obtain in-situ, epitaxially grown Lu doped YBCO thin films with good superconducting properties by PLD, two parameters have to be controlled: the substrate temperature both during deposition and annealing and the oxygen partial pressure during the whole

process. The oxygen pressure used during PLD process determines the occupancy of the oxygen sites of the tetragonal phase of the films, whereas the in-situ cooling process determines the occupancy of the oxygen chains of the orthorhombic, superconducting phase. Both effects seem to be independent from each other. The tetragonal to the superconducting orthorhombic phase transition takes place during a slow cooling under a high oxygen pressure. Our successful parameters are shown in Table 3.1.

We have analyzed the morphological features of our Lu doped YBCO thin films by scanning electron microscopy (SEM), the crystallographic microstructure by X-ray diffraction (XRD), and the superconducting properties of the films by resistance versus temperature measurements. XRD analysis was performed using Phillips X'Pert Pro X-ray diffractometer with Cu-K α $\lambda=1.5418$ Å. The samples were detected with the angles between 5 to 80 degrees. The energy dispersive x-ray spectroscopy (EDX) of the Lu doped YBCO target was performed to observe the chemical ratios of the components of the target. SEM analysis was done by using Phillips XL-380S FEG. The roughness of the film surface was examined by Atomic Force Microscopy (AFM), and the images were taken from a Multimode SPM, Nanoscope IV Digital Instrument. According to SEM results, several round white spots known as laser droplets were lying along the film surface. These laser droplets are a major problem in PLD process and it is not easy to cope with them, and substrate temperature, laser fluence, oxygen pressure are highly relevant to this particulation.

After giving the results of the surface characterization of our samples, the electrical characterization has to be discussed to find out superconducting parameters of the samples. R-T measurements were carried out for this purpose. Four point contact method was applied to the film surface by using silver paint and the measurement was carried out by the help of helium closed-cycle cryostat. By examining R-T graph shown in chapter 4, we found out that transition temperature changes slightly according to annealing time of samples in oxygen pressure and annealing temperature. Two parameters that explained in chapter 4 gave two different transition temperature values such as 82 K and 83.5 K. According to the literature, these transition temperature values are under the YBCO's common transition temperature observed in its thin films. This result might be because our samples may need more oxygenation during the in-situ annealing process.

Consequently, in the end of this study, we produced a stoichiometric target to use in pulsed laser deposition technique. Optimization of PLD took lasts of time and we

tried many parameters in order to obtain usefull parameters for our deposition system. Lutetium doped YBCO thin films were doped on single crystal MgO substrates and their R-T measurement were done. To investigate the effect of Lutetium doping we have to measure the critical current density but we couldn't cope with the particulation on the film surface and we couldn't perform the photolithography process for device patterning. The off-axis geometry might be improved to deal with this major problem in PLD grown films.

REFERENCES

- Abrikosov, A. A. "On the Magnetic Properties of Superconductors of the Second Group." *Theoretical Physics* 32 (1957): 1442-1452.
- Afonso, C.N., J. Gonzalo, R. Serna, J. Solis. "Pulsed Laser Deposition for Functional Optical Films." *Optical Science* 129 (2007): 315-319.
- Afonso, C.N., R. Serna, F. Catalina, D. Bermejo. "Good-quality Ge films grown by excimer laser deposition." *Applied Surface Science* 46 (1990): 249-253.
- Anderson, P.W. "*The Theory of Superconductivity in the High-Tc Cuprates.*" New Jersey: Princeton University Press, 1997.
- Ayache, J. "Grain boundaries in high temperature superconducting ceramics." *Philosophical Magazine*, 86 (2005): 2193-2239.
- Alecu, G. "Crystal structures of some high-temperature superconductors." *Romanian Reports in Physics* 56 (2004): 404-412.
- "Applied Superconductivity Josephson Effects and Superconducting Electronics." Last modified December 12, 2010, http://www.wmi.badw.de/teaching/Lecturenotes/AS/Introduction_2009.pdf.
- Aziz M. J. "Film Growth Mechanisms in Pulsed Laser Deposition." *Applied Physics A* 93 (2008): 579-587.
- Bardeen, J., L. N. Cooper, J. R. Schrieffer. "Microscopic theory of superconductivity." *Phys. Rev.* 106 (1957): 162-164.
- Bean, C.P. "Magnetization of Hard Superconductors" *Phys. Rev. Lett.* 8 (1962): 250-253.
- Bean, C.P." Magnetization of High-Field Superconductors" *Rev. Mod. Phys.* 36 (1964): 31-39.
- Beasley, M. R. "High-temperature superconductive thin films." *Proceedings of the IEEE* 77 (1989): 1155-1161.

- Beasley, M. R. "High temperature superconducting thin films." *Proceedings of the IEEE* 77 (1999): 1155-1163.
- Bednorz, J.G., K.A. Muller. "Possible High T_c Superconductivity in the Ba-La-Cu-O system." *Z. Phys. B.* 64 (1986): 189-193.
- Boffa, V., T. Petrison, L. Ciontea, U. Gambardella, S. Barbanera. "High-quality surface YBCO thin films prepared by off-axis pulsed laser deposition technique." *Physica C: Superconductivity* 276 (1997): 218-224.
- Braginski, Alex, J. Krause and J. Vrba. *Handbook of thin film devices*. New York: Academic, 2000.
- Branescu, M., V.S. Teodorescu, G. Socol, I. Balasz, C. Ducu, and J. Jaklovszky. "Experiments on pulsed laser deposition and characterization of epitaxially in situ grown $\text{YBa}_2\text{Cu}_3\text{O}_{7-\delta}$ thin films." *Journal of Optoelectronics and Advanced Materials* 7 (2005): 967-972.
- Branescu, Maria, A. Vailionis, I. Ward, J. Huh, G. Socol. "In situ grown epitaxial $\text{YBa}_2\text{Cu}_3\text{O}_{7-\delta}$ thin films by pulsed laser deposition under reduced oxygen pressure during cool-down time." *Applied Surface Science* 252 (2006): 4573-4577.
- Branescu, M., A. Vailionis, J. Huh, A. Moldovan, and G. Socol. "AFM and complementary XRD measurements of *in situ* grown YBCO films obtained by pulsed laser deposition." *Applied Surface Science* 253 (2007): 8179-8183.
- Branescu, M., I. Ward, J. Huh, Y. Matsushita, and G. Zeltzer. "Scanning electron microscopy and resistive transition of *in-situ* grown YBCO films by pulsed laser deposition." *Journal of Physics: Conference Series* 94 (2008) 012007. doi:10.1088/1742-6596/94/1/012007.
- BZel'dovic, Ya., Yu.P.Raizer. *Physics of shock waves and high temperature hydrodynamic phenomena*. New York: Academic Press, 1966.
- Cava, R. J. "Oxide superconductors", *J. Am. Ceram. Soc.* 83 (2000): 5-28.

- Chaudhari, P., J. Mannhart, and D. Dimos. "Direct measurement of superconducting properties of single grain boundaries in YBCO." *Physics Review Letters* 60 (1998): 1653-1656.
- Chen, Kuen-Lin, Jau-Han Chen, Hong-Chang Yang, and Heng-Er Horng. "Off-axis pulsed laser deposited $\text{YBa}_2\text{Cu}_3\text{O}_{7-\delta}$ thin films for device applications." *Physica C: Superconductivity* 372-376 (2002): 1078-1081.
- Chu, C. W., J. Bechtold, L. Gao, P. H. Hor, Z. J. Huang, R. L. Meng, Y. Y. Sun, Y. Q. Wang, and Y. Y. Xue "Superconductivity up to 114 K in the Bi-Al-Ca-Sr-Cu-O compound system without rare-earth elements." *Phys. Rev. Lett.* 60 (1988): 941-943.
- Chrzanowski, J., S. Meng-Burany, W. Xing, A. E. Curzon, B. Heinrich, J. C. Irwin, R. A. Cragg, Hu. Zhou, F. Habib, V. Angus, and A. A. Fife. "Optimization of the deposition conditions and structural characterization of $\text{YBa}_2\text{Cu}_3\text{O}_{7-\delta}$ thin superconducting films." Paper presented at the conf. proc. of the 4th World Congress on Superconductivity, Orlando, Florida, USA, June 27-July 1, 1994.
- Chrzanowski, J., D. Atlan, W. Xing, F. Habib, B. Heinrich, J. C. Irwin, R. A. Cragg, Hu. Zhou, F. Habib, V. Angus, and A. A. Fife. "Correlations between critical current density, j_c , critical temperature, T_c , and structural quality of $\text{YBa}_2\text{Cu}_3\text{O}_{7-\delta}$ thin superconducting films." Paper presented at the proc. of the 4th World Congress on Superconductivity, Orlando, Fla., USA, June 27-July 1, 1994.
- Cogollo, R.P., A. C. Marino, and H. M. Sanchez. "Transport properties of YBCO superconducting films at different oxygen concentration." *IEEE Trans. on Appl. Supercond* 13 (2003): 2789-2791.
- Chrisey, D. B., G. K. Hubler. *Pulsed Laser Deposition of Thin Films*. New York: Willey, 1994.
- Chudzik, Micheal Patrick. "Crystalline Orientation Engineering and Charge Transport in Thin Film $\text{YBaCu}_3\text{O}_{7-\delta}$ Superconducting Surface-Coated Conductors." PhD thesis, Northwestern University, 2000.

- Dahl, Per Fridtjof. *Superconductivity: Its Historical Roots and Development from Mercury to the Ceramic Oxides*. New York: American Institute of Physics, 1992.
- De Gennes, P.G. "Boundary Effects in Superconductors." *Review Modern Physics* 36 (1964): 225-237.
- Dijkkamp, D., T. Venkaatesan, X. D. Wu, S. A. Shaheen, N. Jisrawi, Y. H. Min-Lee, W. L. Mclean, and M. Croft. "Preparation of Y-Ba-Cu oxide superconductor thin films using pulsed laser evaporation from high T_c bulk material." *Applied Physics Letters* 51 (1987): 619-621.
- Djupmyr, Märit. "The Role of Temperature for the Critical Current Density in High-Temperature Superconductors and Heterostructures." PhD thesis, Max-Planck-Institut für Metallforschung, 2008.
- Eason, Robert W. *Pulsed Laser Deposition of Thin Films Applications-Led Growth of Functional Materials*. Chichester, UK: Willey Interscience, 2007.
- Eulenburg, A., E. J. Romans, Y. C. Fan, C. M. Pegrum. "Pulsed laser deposition of $\text{YBa}_2\text{Cu}_3\text{O}_{7-\delta}$ and $\text{NdBa}_2\text{Cu}_3\text{O}_{7-\delta}$ thin films: a comparative study." *Physica C* 312 (1999): 91-104.
- Farhat, L. Ben, M. Amami, E. K. Hlil, R. Ben Hassen. "Synthesis, structure and magnetic properties of the $\text{Lu}_2\text{O}_3\text{-CoO}$ mixed system." *Materials Chemistry and Physics* 123 (2010): 737-741.
- Fossheim, K., and A. Sudbo. *Superconductivity Physics and Applications*. England: John Wiley & Sons Ltd, 2004.
- Gross, R., L. Alf, and A. Beck. "Physics and Technology of high temperature superconducting Josephson junctions." *IEEE Transactions of Applied Superconductivity* 7 (1997): 2929-2935.
- Hakola, Antti. "Thin-film deposition using laser ablation: application to ferromagnetic shape-memory materials and methods for spatial shaping of laser beams." PhD diss., Helsinki University of Technology, 2006.

- Hazen, Robert M. *The breakthrough: the race for the superconductor*, New York: Summit Book, 1988.
- Hilgenkamp H., and Mannhart J. “Grain Boundaries in high- T_c superconductors.” *Review of Modern Physics* 74 (2002): 485-549.
- Huhtinen, H., P. Paturi, E. Lähderanta, R. Laiho, J. Raittila, and Yu. Stepanov. 1999. “YBCO nanopowder: novel material for PLD preparation of thin films.” *Physica C: Superconductivity* 341-348 (2000): 2377-2378.
- Huijben, M. “Tuning electronic properties by atomically controlled growth.” PhD Thesis, University of Twente, 2006.
- H. Ibach and H. Lüth. *Solid-State Physics - An Introduction to Principles of Materials Science*. Berlin: Springer-Verlag, 1996.
- Ibach, H., H. Lüth. *Solid-State Physics*. Berlin: Springer, 1995.
- Jorgensen, J. D., M. A. Beno, and D. G. Hinks. “Oxygen ordering and the orthorhombic to tetragonal phase transition in YBCO.” *Physical Review B* 36 (1987): 3608-3616.
- Kim, Cheol-Su, Sung-Min Kim, Seok-Cheon Song, Sang Yeol Lee, Hyung Kuk Yoon, Young Joong Yoon. “Fabrication and characterization of a superconducting multiplexer using laser ablated YBCO thin films.” *Applied Surface Science* 154-155 (2000): 492-494.
- Kim, Sungwook. “The Proximity Effects in High Temperature Superconductor Nano Structures.” PhD thesis, The University of Texas, 2005.
- Kittel, C. *Introduction to Solid State Physics*. New York: John Wiley and Sons, 1996.
- Krebs, H. U., Weisheit, M., Sükse, E., Scharf, T., Fuhse, C., Störmer, M., Sturm, K., Seibt, M., Kijewski, H., Nelke, D., Panchenko, D., and Buback, M. “Pulsed Laser Deposition (PLD) - a Versatile Thin Film Technique”, *Advances in Solid State Physics Springer* 43 (2003): 101–107.

- Kresin, V.Z., and S.T. Wolf. *Fundamentals of superconductivity*. New York, USA: Plenum Publishing, 1990.
- Kunold, A., M. Hernandez, A. Myszkowski, J. L. Cardoso, and P. Pereyra. "AC susceptibility in granular superconductors: theory and experiment." *Physica C: Superconductivity* 370 (2002): 63-70.
- Lewis, B., J. C. Anderson. *Nucleation and Growth of Thin Films*. New York: Academic Press, 1978.
- Liu, Lihua, Cheng Dong, Jincang Zhang, Hong Chen, Ling Chen. "A simple volumetric method for oxygen content determination in high- T_c doped YBCO compositions." *Physica C* 383 (2002): 17-22.
- Lumpp, J. K., and S. D. Allen. "Excimer laser machining and metallization of vias in aluminum nitride." *IEEE Transactions on Components Packaging and Manufacturing Technology Part B: Advanced Packaging* 20 (1997): 241-246.
- "Magnesium Oxide," last modified December 12, 2010,
http://www.webelements.com/compounds/magnesium/magnesium_oxide.html.
- Malisa, Anayesu. "Magnesium Diboride (MgB_2) and Ca-doped $YBa_2Cu_3O_{7-\delta}$: Thin Films and Devices Fabrication and Characterization." PhD thesis, Chalmers University of Technology, 2005.
- Mathis, J.E., Christen, H.M. "Factors that influence particle formation during pulsed electron deposition of YBCO precursors" *Physica C* 459 (2007): 47-51.
- Murakami, M. "Processing of bulk YBCO." *Supercond. Sci. Technol.* 5 (1992): 185-203.
- Ohring, M. *The Materials Science of Thin Films*. San Diego: Academic Press, 1992.
- Orlando, Terry P. and Kevin A. Delin. *Foundations of Applied Superconductivity*. New Jersey: Prentice Hall, 1991.

- Öztürk, Ali, İbrahim Düzgün, Selahattin Çelebi. "The effect of partial Lu doping on magnetic behaviour of YBCO (123) superconductors." *Journal of Alloys and Compounds* 495 (2010): 104-107.
- Parinov, I. A. *Microstructure and Properties of High-Temperature Superconductors*. New York: Springer, 2007.
- Park, Joo Hyung, Sang Yeol Lee. "Fabrication and characterization of double-sided YBCO superconducting thin films using laser ablation." *Surface and Coating Technology* 113 (1999): 274-277
- Peacor, S. D., C. Uher, A. H. Francis, J. Shewchun. "Physical and electromagnetic properties of Y-Ba-Cu-O superconductors synthesized with peroxides." *Journal of Applied Physics* 67 (1990): 7488- 7492.
- Peterlongo, A., A. Miotello, and R. Kelly. "Laser-pulse sputtering of aluminum: Vaporization, boiling, superheating, and gas-dynamic effects." *Phys. Rev.* 50 (1994): 4716-4727.
- Phillips, J. "Substrate selection for high temperature superconducting thin films." *Journal of Applied Physics* 79 (1996): 1829-1833.
- Poole, C. P. *Copper Oxide Superconductors*. New York: Wiley-Interscience Publications, 1998.
- Poole, C. P. *Handbook of Superconductivity*. USA: Academic Press, 2000.
- Rajiv, K.S., D. Kumar. "Pulsed laser deposition and characterization of high-T_c YBCO superconducting thin films." *Material Science and Engineering* 22 (1998): 113-185.
- Ready, J. F. "Development of plume of material vaporized by giant-pulse laser." *Applied Physics Letters* 3 (1963): 11-13.
- Ready, J.F. *Effects of High - Power Laser Radiation*. New York: Academy Press, 1971.
- Rijnders, G. "The initial growth of complex oxides: study and manipulation." PhD Thesis, University of Twente, 1999.

- Seeber, B. *Handbook of applied superconductivity*. Bristol, UK: Inst. Phys. Publishing, 1998.
- Schlepütz, Christian M., "Systematic Structure Investigation of YBCO Thin Films with Direct Methods and Surface X-ray Diffraction." PhD thesis, University of Zurich, 2009.
- Schrieffer, J. R. *Theory of Superconductivity*. Florida: Westview Press, 1995.
- Schuegraf, K. K. *Handbook of thin-film deposition process and Applications*. New Jersey, USA: Noyes Publications, 1988.
- Seshan, K. *Handbook of Thin-Film Deposition Processes and Techniques - Principles, Methods, Equipment and Applications*. New Jersey, USA: Noyes Publications, 2002.
- Sheahen, T. P. *Introduction to High Temperature Superconductivity*. New York: Plenum Press, 1994.
- Shi, D. *High Temperature Superconducting Materials*. New York: Pergamon, 1995.
- Simon, Randy, and Andrew Smith. *Superconductors: Conquering Technology's New Frontier*. New York and London: Plenum Press, 1988.
- Singh, Rajiv K., D. Kumar. "Pulsed laser deposition and characterization of high-T_c YBa₂Cu₃O_{7-x} superconducting thin films." *Materials Science and Engineering* 22 (1998): 113-185.
- Smith, D. J. *Thin-Film Deposition: Principles and Practice*. Boston: McGraw-Hill, 1995.
- Soltan, Soltan Eid Abdel-Gawad. "Interaction of Superconductivity and Ferromagnetism in YBCO/LCMO Heterostructures." PhD thesis, Max-Planck-Institut Festkörperforschung, 2005.
- Suh, J. D., G. Y. Sung, K. Y. Kang, H. S. Kim, J. Y. Lee, D. K. Kim, C. H. Kim. Cubic Y-Ba-Cu-O thin films by high speed pulsed laser deposition. *Physica C* 308 (1998): 251-256.

- Tinkham, Michael. *Introduction to Superconductivity*. New York: McGraw Hill, 1990.
- Tuohiniemi, M. "Laser-Ablation System for Depositing High-Temperature Superconducting YBaCuO Thin Films." Master's Thesis, Helsinki University of Technology, 1999.
- Uchiyama, T., I. Iguchi. "Control of crystal orientation in YBCO thin films by an oxygen diffusion process." *Supercond. Sci. Technol.* 17 (2004): 592-595.
- Wesche, R. *High-Temperature Superconductors: Materials, Properties and Applications*. London: Kluwer Academic Publishers, 1998.
- Wördenweber, R. "Growth of high-Tc thin films." *Superconductor Science and Technology* 12 (1999): 86-102.
- Wu, M. K., J. R. Ashburn, C. J. Torng, P. H. Hor, and R. L. Meng. "Superconductivity at 93 K in a new mixed-phase Y-Ba-Cu-O compound system at ambient pressure." *Physical Review Letters* 58 (1987): 908-910.
- Xing, W. B. Heinrich, J. Chrzanowski, J. C. Irwin, H. Zhou, A. Cragg, and A. A. Fife. "Determination of critical current densities of YBa₂Cu₃O_{7-δ}-d thin films from ac susceptibility measurements." *Physica C* 205 (1993): 311-322.
- Yahya, N., H. G. Beh, M. Hashim. "Development of Pulsed Laser Deposition System for the Formation of Web-liked Carbon Nanotubes." *American Journal of Applied Sciences* 2 (2005): 1509-1515.